Biomaterials Science

ROYAL SOCIETY OF CHEMISTRY

REVIEW

View Article Online
View Journal | View Issue

Check for updates

Cite this: *Biomater. Sci.*, 2023, **11**, 4430

Microneedles: a novel strategy for wound management

Ze Qiang Zhao,[a,b] Ling Liang,[a,b] Li Yue Jing,[a,b] Yue Liu,[a,b] Yu Han Zhang,[a,b] Mohammad-Ali Shahbazi, *[c,d,e] Bo Zhi Chen*[a,b] and Xin Dong Guo *[a,b]

Wound management is a serious concern worldwide, inflicting a huge social and economic burden on patients and healthcare systems, and research into efficient wound-management measures is crucial. Although advances have been made in traditional wound dressings for wound management to date, the complicated environment near the wound leads to inadequate drug absorption for achieving the intended therapeutic impact. Microneedles, a novel transdermal drug delivery method, can improve wound-healing efficacy by breaking down the barriers at the wound site and enhancing drug delivery efficiency. In recent years, there have been many advanced types of research on the application of microneedles to wound management to address the difficulties encountered in the wound-healing process. This article summarizes and analyzes these research efforts, classifying them according to their distinct efficacy, and addresses them in five areas: hemostasis, antibacterial effects, proliferation, anti-scar, and wound monitoring. The article concludes with a review of the current state and limitations of microneedle patches and an outlook on the future direction of microneedles in wound management as a way to inspire more efficient and smarter wound-management strategies.

Received 16th February 2023,
Accepted 22nd April 2023

DOI: 10.1039/d3bm00262d

rsc.li/biomaterials-science

Published on 03 mai 2023. Downloaded on 05.06.2026 15:09:01.

1. Introduction

As the body's biggest organ, the skin is in direct contact with the external world and serves as the first line of defense against external stimuli.[1] Various types of skin damage can result in the formation of skin wounds. Even though these wounds can normally slowly heal, the healing process results in the production of scars and the loss of skin appendages such as sweat glands and hair.[2,3] In addition, some acute wounds resulting from physical injury require rapid hemostasis and immobilization to prevent microbial infection during the healing period.[4,5] If the patient has diabetes, cancer, or other diseases, this will delay the wound-healing cycle and create a chronic wound, resulting in long-term harm to the patient's body and psyche.[6–8]

To avoid potential injury from anomalies in the wound-healing process, billions of dollars are invested in research each year worldwide to develop more effective wound-treatment procedures.[9,10] To better comprehend the current wound-management measures, we need to first understand the process and mechanism of wound healing. As shown in Fig. 1, the normal wound-healing process includes four phases: hemostasis, inflammation, proliferation, and remodeling.[11,12] After the skin is damaged, blood pours out of the wound to flush away pathogens, and vasoconstriction begins the hemostatic process. During this process, platelets are triggered to bind with fibrin to produce a fibrin clot, which acts as a hemostatic agent while providing a temporary infiltration site for the subsequently recruited inflammatory cells.[13–15] As neutrophils and monocytes are drawn to the wound site, the wound heals into the inflammatory phase to clear dead cells, damaged tissue, and infecting bacteria. During the initial phase of inflammation, neutrophils release chemokines (CC and CXC subfamilies) and pro-inflammatory cytokines (tumor necrosis factor-α (TNF-α), interleukin-1 (IL-1) and interleukin-6 (IL-6)) to amplify the immune response and induce monocytes to differentiate to macrophages to continue clearing debris.[16–18] During the inflammatory phase, macrophages are pro-inflammatory cells of the M1 phenotype, but as the cleanup is completed and the inflammatory signal diminishes, macrophages gradually differentiate into the anti-inflammatory M2 phenotype and secrete growth factors to

[a]*State Key Laboratory of Organic–Inorganic Composites, Beijing University of Chemical Technology, Beijing 100029, China. E-mail: xdguo@buct.edu.cn*
[b]*Beijing Laboratory of Biomedical Materials, College of Materials Science and Engineering, Beijing University of Chemical Technology, Beijing 100029, China. E-mail: chenbz@buct.edu.cn*
[c]*Department of Biomedical Engineering, University Medical Center Groningen, University of Groningen, Antonius Deusinglaan 1, 9713 AV Groningen, The Netherlands. E-mail: m.a.shahbazi@umcg.nl*
[d]*W.J. Kolff Institute for Biomedical Engineering and Materials Science, University of Groningen, Antonius Deusinglaan 1, 9713 AV Groningen, The Netherlands*
[e]*Department of Pharmaceutics, School of Pharmacy, Zanjan University of Medical Science, 45139-56184 Zanjan, Iran*

This journal is © The Royal Society of Chemistry 2023

Published on 03 mai 2023. Downloaded on 05.06.2026 15:09:01.

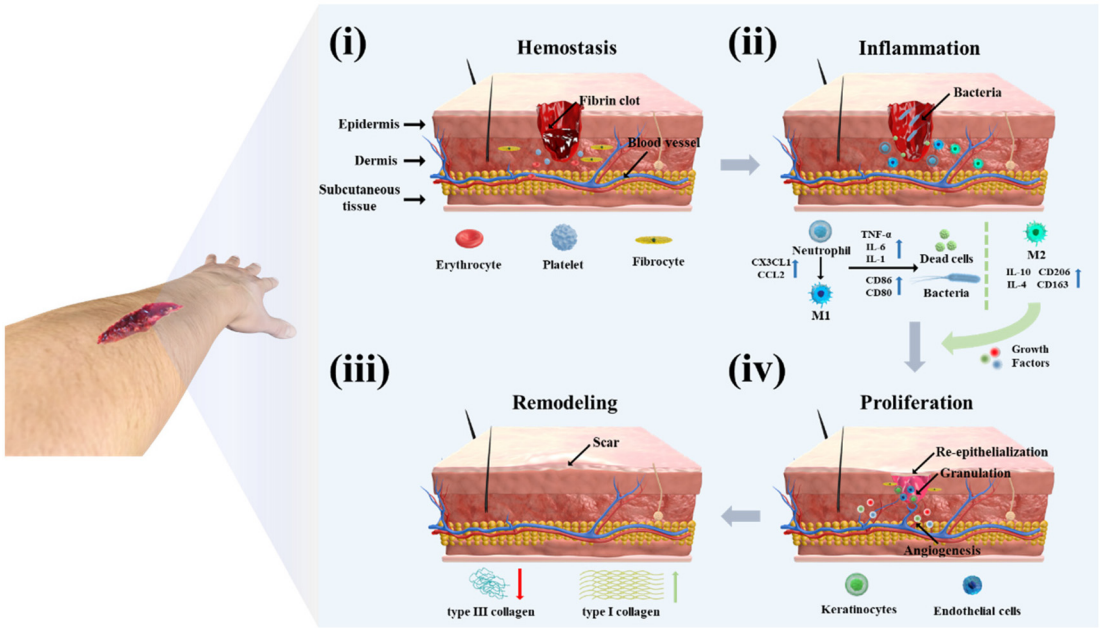

Fig. 1 The mechanisms and procedures involved in wound healing. (i) Hemostasis: platelets combine with fibrin to form a fibrin clot to achieve rapid hemostasis; (ii) inflammation: secretion of pro-inflammatory factors, recruitment of verified cells at the wound, and clearance of cellular debris and foreign bacteria; (iii) proliferation: transformation of immune cells from pro-inflammatory to anti-inflammatory type, secretion of growth factors, promotion of angiogenesis, granulation tissue formation, and re-epithelialization; (iv) remodeling: gradual degradation of type III collagen to form a more neat type I collagen.

attract various cells to the wound for repair, which in turn leads to wound healing into the proliferative phase.[15] There are three key signature events throughout the proliferative phase: angiogenesis, granulation tissue formation, and re-epithelialization.[19] During this phase, to ensure cellular activity during proliferation, angiogenic factors (VEGF, PDGF, and PGF) induce the construction of blood vessels at the wound site to ensure the delivery of oxygen and nutrients.[20,21] At the same time, encouraged by cytokines, fibroblasts, keratinocytes, and endothelial cells multiply and differentiate to generate light pink granulation tissue to provide a framework for extracellular matrix (ECM), blood vessels, and inflammatory cells.[22,23] At the same time, basal cells from the faulty tissue migrate to the wound surface to multiply in huge numbers to eventually form epithelial cells in re-epithelialization.[24] Subsequently, the remodeling phase of wound healing

Ze Qiang Zhao

Ze Qiang Zhao obtained his M.S. degree from the Beijing University of Chemical Technology (BUCT) in 2022. He is a PhD student in Prof. Guo's group at the Microneedle Research Center, School of Materials Science and Engineering, BUCT. His recent work mainly focuses on microneedles for autoimmune diseases.

Mohammad-Ali Shahbazi

M.-A. Shahbazi received his Ph.D. in 2015 from the University of Helsinki, Finland, before moving to the Technical University of Denmark to develop lab-on-a-chip devices for sepsis diagnosis. He then worked as an Academy of Finland Fellow on microimplants for the treatment of autoimmune disorders. He is currently an assistant professor at the University Medical Center Groningen, The Netherlands, and the co-founder of Capsamedix Oy Company. Dr Shahbazi has plenty of experience in drug delivery systems and he aims to shape the future of multifunctional medicines through the combination of materials science, biology, nanotechnology, and medical devices.

Published on 03 mai 2023. Downloaded on 05.06.2026 15:09:01.

starts. During this phase, the type III collagen deposited during the previous healing process is gradually degraded and transformed into a more neatly ordered type I collagen.[22] At this time, the skin slowly regains its elasticity and some functionality, such as the transformation of capillaries into more stable arteries or veins and the regeneration of hair, sweat, and sebaceous glands.

However, in most wounds, the healing process is confronted by numerous impediments that lead to slow or even problematic wound recovery. During the hemostasis stage, to protect the wound site from the external environment, airtight treatment of the wound is essential to avoid infection of the wound in the complex environment.[2,6,15] However, traditional therapies, such as sutures and staples, might lead to excessive local mechanical stress eventually producing scars.[25,26] Some individuals with coagulation abnormalities or in the presence of deep wounds also require human intervention to rapidly stop bleeding to avoid the detrimental consequences of excessive blood loss. Although the body's immune system clears microorganisms to prevent infection during the inflammatory phase, the complicated environment will undoubtedly lead to unanticipated scenarios. Wounds are commonly accompanied by biofilms tens or even hundreds of microns thick, providing a suitable breeding ground for microbial invasion. On the one hand, bacterial biofilms can restrict the penetration impact of medications, and on the other hand, a complex microbial environment can lead to microbial antibiotic resistance, which in turn leads to prolonged infection and poor wound healing.[27–29] In some diabetic and cancer patients, high levels of reactive oxygen species (ROS) and persistent inflammation can lead to low expression of growth factors associated with the proliferative phase, which in turn leads to impaired angiogenesis and difficulties in transporting nutrients and oxygen to the wound site, resulting in long-term difficulties in wound repair and, in severe cases, skin ulceration.[30,31] In addition, inappropriate behavior during the wound-healing process, especially during the inflammatory and proliferative stages, can lead to excessive fibroblast proliferation and an imbalance in collagen synthesis and degradation, resulting in ineffective wound healing and ultimately scar formation.[32]

To cope with the diverse conditions encountered in the wound-healing process, a great number of different types of wound dressings have been developed in recent years for the treatment of wounds at different stages. These wound dressings can be categorized into four main types according to their functionality: (1) hemostatic wound dressings that improve adhesion and activate platelet coagulation;[23,33] (2) antimicrobial wound dressings that are loaded with antibiotics and other antimicrobial drugs, sterilized by photothermal or photodynamic conversion, or cationic polymeric materials with antimicrobial properties;[34,35] (3) wound dressings that deliver small molecules such as oxygen, nitric oxide, anti-inflammatory drugs, reparative cell signaling factors, and even exosomes and stem cells used to reduce the inflammatory response, induce the healing phase into the proliferative phase, and enhance the generation of blood vessels;[36,37] (4) wound dressings for determining wound-healing status by detecting pH, glucose, temperature, and hydrogen peroxide.[32,38–40] However, during the wound-healing process, the wound site secretes fibrin, thrombin, and other secretions to form a fibrin clot to protect the wound from the external environment, but at the same time, this slows the penetration rate of the therapeutic compounds in the dressings and drastically reduces the utilization of the drug.[41,42] In the case of severe bacterial infections, the thicker bacterial biofilm can hinder the therapeutic effect of the antibiotic dressings, leading to long-term infection or even ulceration of the wound.

Microneedle (MN) patches are a novel form of transdermal drug delivery in which therapeutic drugs are efficiently delivered transdermally by penetrating these protective layers in a minimally invasive way with a needle body of hundreds of micrometers in height.[43–47] To date, various matrix materials have been employed to fabricate MNs,[48–52] including polylactic

Bo Zhi Chen

Bo Zhi Chen currently works at the College of Materials Science and Engineering, Beijing University of Chemical Technology (BUCT). He studied as a joint doctoral student at Osaka University in 2019 and received his Ph.D. degree from BUCT in 2021. His research focuses on biomaterials for biomedical applications, polymer microneedles-based systems for controlled drug delivery, and wearable biosensors for diagnosis.

Xin Dong Guo

Xin Dong Guo is currently a full professor at the College of Materials Science and Engineering and Dean of the High-Tech Research Institute at Beijing University of Chemical Technology (BUCT), PR China. He received his Ph.D. in Chemical Engineering from the South China University of Chemical Technology, followed by postdoctoral experience at Georgia Tech. In 2013, he joined BUCT as a full professor. His research interests include controlled drug delivery, biosensors, microneedles and nanobiotechnology.

This journal is © The Royal Society of Chemistry 2023

Published on 03 mai 2023. Downloaded on 05.06.2026 15:09:01.

acid (PLA), silicon, stainless steel, and light-curing resin for generating MNs. Polyvinyl alcohol (PVA), hyaluronic acid (HA), silk protein, and gelatin have been utilized to form soluble MNs, while gelatin methacryloyl (GelMA), hyaluronic acid methacryloyl (HAMA), and sodium alginate have been employed to form hydrogel MNs. The fabrication techniques, including laser engraving, 3D printing, and template-based preparation, can be utilized to create MNs from the above diverse materials. MN technology has gained widespread use over the last 15 years in a variety of applications, including dermatological treatment,[53] vaccine delivery,[54,55] insulin administration,[45,56,57] and stem cell transplantation.[58] Unlike traditional transdermal drug delivery methods, MNs can permeate the skin in a non-invasive and pain-free manner, thereby enhancing drug absorption and utilization. The customizable structure and composition of MNs allow for smart response,[59,60] controlled drug release,[61,62] multi-drug therapy,[63–65] and targeted delivery to specific sites, such as the gut,[66] heart,[67] blood vessels,[68] and brain.[69] MNs are also widely used in biomonitoring. Compared with traditional detection dressings, the needle body of MNs can directly contact with the skin interstitial fluid at the wound to detect glucose, cholesterol, uric acid, sodium ions, pH, *etc.*,[70–73] and the detection is more sensitive and the results are more accurate.

In recent years, MNs have made tremendous progress in the field of wound-healing applications. In this article, these works are organized and divided according to the different roles played by MNs in the wound-healing process, and their advantages and disadvantages are analyzed and discussed. At the conclusion of the article, the key points of the review are summarized, along with some current limitations and future directions for the field.

2. Microneedles for wound management

In wound management, wound crusting can hinder drug absorption and impair therapeutic efficacy. MNs have been shown to overcome this challenge by enhancing drug absorption and patch adhesion through hundreds of micron-sized needles. In addition to improving the efficiency of drug utilization to improve the therapeutic effect, the matrix material and needle structure of MN patches can be adjusted to improve their adhesion and hemostatic ability in the early wound.[74–76] A large number of studies have found that the matrix material of MNs has a protective effect on protein-based drugs, sRNA, exosomes, and even stem cells loaded in MNs, which can maintain their activity over time.[58] In addition, by designing the MN structure, the rapid separation of the needle body from the backing layer can be achieved, enabling the rapid implantation of the drug-delivery portion in the wound and avoiding the combination of new tissue with the dressing at the later stage of treatment, which can bring secondary damage during removal. Additionally, the ability of MNs to facilitate direct detection of the wound microenvironment *via* interstitial fluid provides insight into the wound-healing process. There has been growing interest in MNs for wound management in recent years, with research exploring various functionalities, including hemostasis, antibacterial, proliferation, anti-scar, and wound monitoring. This review provides a comprehensive overview of previous studies and aims to stimulate the development of advanced and intelligent wound-management strategies using MNs.

2.1 Microneedles for hemostasis

The human body often experiences bleeding after some physical and chemical shocks, bringing great losses to the economy and society, and it is necessary to achieve rapid and efficient hemostasis.[77] The first stage in the wound-healing process is the hemostasis period. Following a vascular injury, vascular contraction occurs to reduce blood loss, and platelets adhere to the injured tissue endothelium, activating to form platelet plugs for rapid hemostasis.[78] The coagulation cascade is then initiated and amplified to produce thrombin, which stimulates the conversion of fibrinogen to fibrin and interacts with platelets to form a fibrin clot.[79,80] For uncontrollable bleeding, the current means of hemostasis is mainly to close the wound by human intervention, activate platelets through hemostatic material recruitment and stimulate the cascade reaction to promote coagulation. The moist environment resulting from blood can present challenges for the adhesion of hemostatic materials, making it a focus of ongoing hemostasis research to enhance both adhesion and hemostasis.

In the initial stage of hemostasis, rapid wound closure is required, and conventional sutures and staples cause tissue damage, inflammation, and other side effects.[81,82] To solve this problem, Jeon *et al.* developed swellable hydrogel-forming double-layered adhesive MNs inspired by endoparasites.[75] As shown in Fig. 2a(i), the MNs have an inner core of filamentous protein and an outer shell of mussel adhesion protein with swelling properties. The internal filamentous protein ensures the mechanical properties of the MNs, and the external mussel adhesive protein rapidly absorbs water and swells after puncture into the skin to achieve mechanical interlocking. In a sealability test, the MNs can withstand a pressure of 139.7 ± 14.1 mm Hg, far exceeding normal human arterial blood pressure. In the wound-healing test, the MN treatment group showed a higher healing effect after 21 days, and the ultimate fracture strength in the wound fracture test was three times higher than that of the sutured group (Fig. 2a(ii)). Besides, this MN bilayer has better biocompatibility and biodegradability. In order to further improve the fixation ability of MNs, the structure of the needle body can be designed. As shown in Fig. 2b, Han *et al.* designed an MN with barbs inspired by organisms in nature.[74] The authors used a digital light-processing 3D printing technique to prepare the MNs. During the preparation process, the resin material is cured under the action of UV radiation, but the upper layer of resin reduces the radiation energy to create a crosslink density gradient within the resin, with a high crosslink density at the top and a low

Published on 03 mai 2023. Downloaded on 05.06.2026 15:09:01.

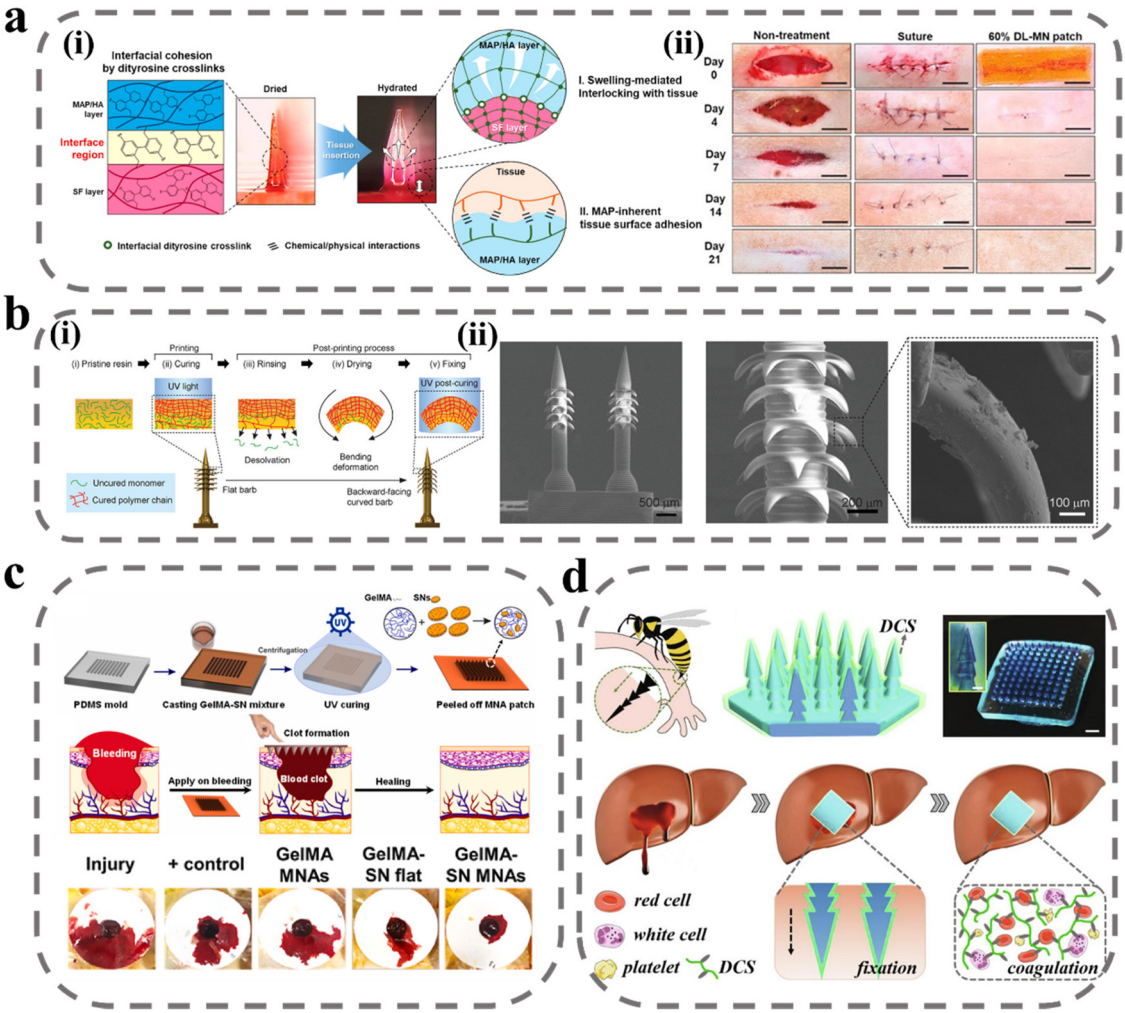

Fig. 2 MNs for wound immobilization and hemostasis. (a) Bio-inspired swellable hydrogel-forming double-layered adhesive MN protein patch for hemostasis: (i) schematic illustration for the proposed working mechanisms of a hydrogel-forming adhesive MN patch; (ii) wound closure and therapeutic effect.[75] Reprinted from the Elsevier, Copyright 2019. (b) Bioinspired MN array with backward-facing barbs: (i) principles for the preparation of MN arrays with backward barbs; (ii) SEM of MN array with backward-facing barbs.[74] Reprinted from the John Wiley and Sons, Copyright 2020. (c) Schematic of GelMA-SN MNs fabrication steps and graphical representation of facile application of GelMA-SN MNs onto a bleeding model to stop hemorrhage.[84] Reprinted from the Elsevier, Copyright 2023. (d) Design and hemostatic function of the bioinspired pagoda-like MN patches.[85] Reprinted from the Elsevier, Copyright 2021.

crosslink density at the bottom with some uncrosslinked monomers. After printing is completed, the MN array is immersed in an organic solvent to extract the uncrosslinked monomers. When the MNs dry the bottom of the barb contracts, causing the barb to bend downward. In the adhesion force test, the tissue adhesion force of MNs with reverse barbs was 18 times higher than that of MNs without barbs.

To improve coagulation at the wound site, fibrinogen and thrombin are considered to be the most effective hemostatic drugs, but they are expensive and have a short shelf life, and are not suitable for mass-production applications.[83] Lee *et al.* used tranexamic acid as an alternative drug to be loaded with soluble hyaluronic acid (HA) MNs at the tip of the needle.[76] Tranexamic acid can specifically bind to tissue fibrinogen activator and inhibit fibrinogen and its fibrin from being degraded, thereby improving the stability of fibrin clots at the wound and improving hemostasis. In the heparin-treated model, the bleeding time and bleeding volume were much lower in the drug-laden MN treatment group than in the non-drug-laden group. The hydrogel material not only helps manage bleeding but also maintains a certain degree of wetness at the wound site, in addition to having better adhesive properties due to the reactive groups in the hydrogel that can react with the proteins in the tissue. Gelatin is widely used for wound hemostasis due to its high biocompatibility, low price, and easy modification. Haghniaz *et al.* used methacrylate-based gelatin as a matrix material to prepare bioadhesive MN patches doped with silicate nanosheets (SNs) (Fig. 2c).[84] SNs have a negative surface charge and a positive edge charge, and attract platelet aggregation through charge

 This journal is © The Royal Society of Chemistry 2023

Published on 03 mai 2023. Downloaded on 05.06.2026 15:09:01.

interaction and activation of coagulation factors. In the liver injury model, bleeding was reduced by 92% in the GelMA-SN MNs treatment group, and the MNs could be degraded *in vivo* within 4 weeks. To further improve the fixation ability of MNs, Zhang *et al.* designed pagoda-type MNs inspired by the honeybee tail stinger (Fig. 2d).[85] The three-layer pagoda conformation further improved the physical interlocking binding force of MNs, and the average detachment force of MNs was above 3 N cm^{-2} in the tissue adhesion force test. In addition, the authors modified the surface of MNs with a dodecyl-modified chitosan coating, whose molecular chain tails could interact with blood cell membranes and cause blood cells to aggregate and coagulate, thus improving the hemostatic ability. When pagoda-shaped MNs were applied to hemorrhage treatment at the liver, kidney, and spleen sites, hemostasis was achieved within seconds after the MNs were pierced. All of the above studies demonstrated that MNs can be successfully applied for wound hemostasis, and demonstrated the selection of materials for the preparation of MNs, in which different drugs can be loaded to enrich coagulation factors, in addition to the designability of the MN structure, which can improve the wound-closure effect and adhesion of the MN patch by physical interlocking.

2.2 Microneedles for antibacterial effects

Bacterial infection is a major factor that hinders wound healing. During the wound-healing process, a biopolymer layer forms at the wound site that is extremely suitable for the growth of external microorganisms, and forms a bacterial biofilm with the infected microorganisms.[86] Bacterial biofilm secretions induce persistent inflammation of the wound, meaning that the delivery of therapeutic agents to the site of action is impeded, prolonging the healing time and posing a significant challenge to wound treatment. The composition and structure of the biofilm create a mechanical barrier that prevents molecules from spreading through the structure to act on the bacterial biofilm and thus inhibit bacterial proliferation. The most effective means of removing the biofilm is through debridement, but it is often difficult to remove and there are recurrent infections and great discomfort to the patient.[87] To break through the biofilm barrier, there are two main directions: one is to break the biofilm structure by physical means such as electric current, plasma, magnetic field, *etc.*,[88] and the other is to prepare a highly permeable delivery system.[89] However, these two means are on the one hand costly to develop, and on the other hand poor in practicality. MNs can deliver antimicrobial drugs to the site of action by disrupting this biofilm with a needle. Arshad *et al.* prepared soluble MNs by using HA/PVP for the delivery of azithromycin.[90] In an *in vitro* drug-release study, azithromycin was rapidly released to 60% within 30 min, allowing the rapid onset of action at the site of infection. In a subsequent rat model of *Staphylococcus aureus* (*S. aureus*) infection, biofilm was largely cleared by treatment with MNs after five days. In addition, some drugs from nature that have inhibitory effects on bacterial infections in wounds, such as catechins from green tea,[91] methylglyoxal from Manuka honey,[92] and kangfuxin from Periplaneta americana,[93] have also been applied to bacterial infections in wounds using MNs and have made good progress.

However, multiple pathogenic colonies have been reported in organisms, which interact with each other and exchange genes, leading to the development of antibiotic resistance.[94,95] To solve this problem, Su *et al.* designed a novel antimicrobial peptide W379 with only eight amino acids (sequence: RRRWWWWV) based on the cathelicidin gene that encodes LL-37 antimicrobial peptide.[96] W379, which vertically forms an amphiphilic structure with a basic charged amino acid at the top and a hydrophobic structural domain at the bottom, can target the cell membranes of Gram-positive and Gram-negative bacteria and cause bacterial death (Fig. 3a). In their experiments, dissolvable MNs were combined with nanofiber dressings to prepare a Janus-type antimicrobial peptide delivery system. The needle body portion of the MNs was prepared by mixing soluble PVP with W379, and the backing layer portion was prepared by the electrostatic spinning technique of F127/PCL core–shell fibers, and the antimicrobial peptide was loaded onto the fiber membrane by electrospray deposition. In an *in vitro* human skin infection model, the MNs system successfully removed a bacteriophage biofilm composed of *Pseudomonas aeruginosa* (*P. aeruginosa*) and methicillin-resistant *Staphylococcus aureus* (MRSA). In another study by Su *et al.*, the formulation of antimicrobial agents was optimized to achieve the antimicrobial effect by using different antimicrobial agents synergistically.[97] The investigators added $AgNO_3$, $Ga(NO_3)_3$, and vancomycin as substitutes for W379 in the Janus-type delivery system described above (Fig. 3b). In addition to inhibiting bacterial division by binding to the bacterial membrane proteins responsible for transport as well as DNA, Ag also interferes with bacterial cellular respiration and disrupts energy production, initiating the bacterial cell death pathway. Ga^{3+} will replace Fe^{3+} to disrupt its residual metabolic processes. Vancomycin is a glycopeptide antibiotic that kills bacteria by interfering with peptidoglycan in the bacterial cell wall structure to interfere with cell wall synthesis and thus inhibit bacterial growth and reproduction. This work provides a good idea for removing the mixed biofilm of multi-drug resistant bacteria and pathogens.

Zn^{2+}, as a metal cationic antimicrobial agent, is effective for avoiding bacterial biofilm resistance. Zn^{2+} can directly contact the cell wall, leading to the disruption of bacterial cell integrity, in addition to catalyzing the production of ROS, which leads to bacterial death.[98] Yao *et al.* designed an array of Zn-MOF encapsulated MNs, as shown in Fig. 3c, where ZIF-8 was encapsulated in a light-cured hydrogel needle body prepared from MeHA, and the antibacterial effect was achieved by releasing ZIF-8 as the hydrogel swelled and degraded after micro-needle piercing into the subcutis.[99] The design of Zn into the MOF structure can increase the specific surface area of the nanomaterial and improve its therapeutic effect when in contact with bacteria. In an *in vitro* antibacterial test, ZIF-8 significantly reduced the survival rate of *E. coli* and *S. aureus*, and

Published on 03 mai 2023. Downloaded on 05.06.2026 15:09:01.

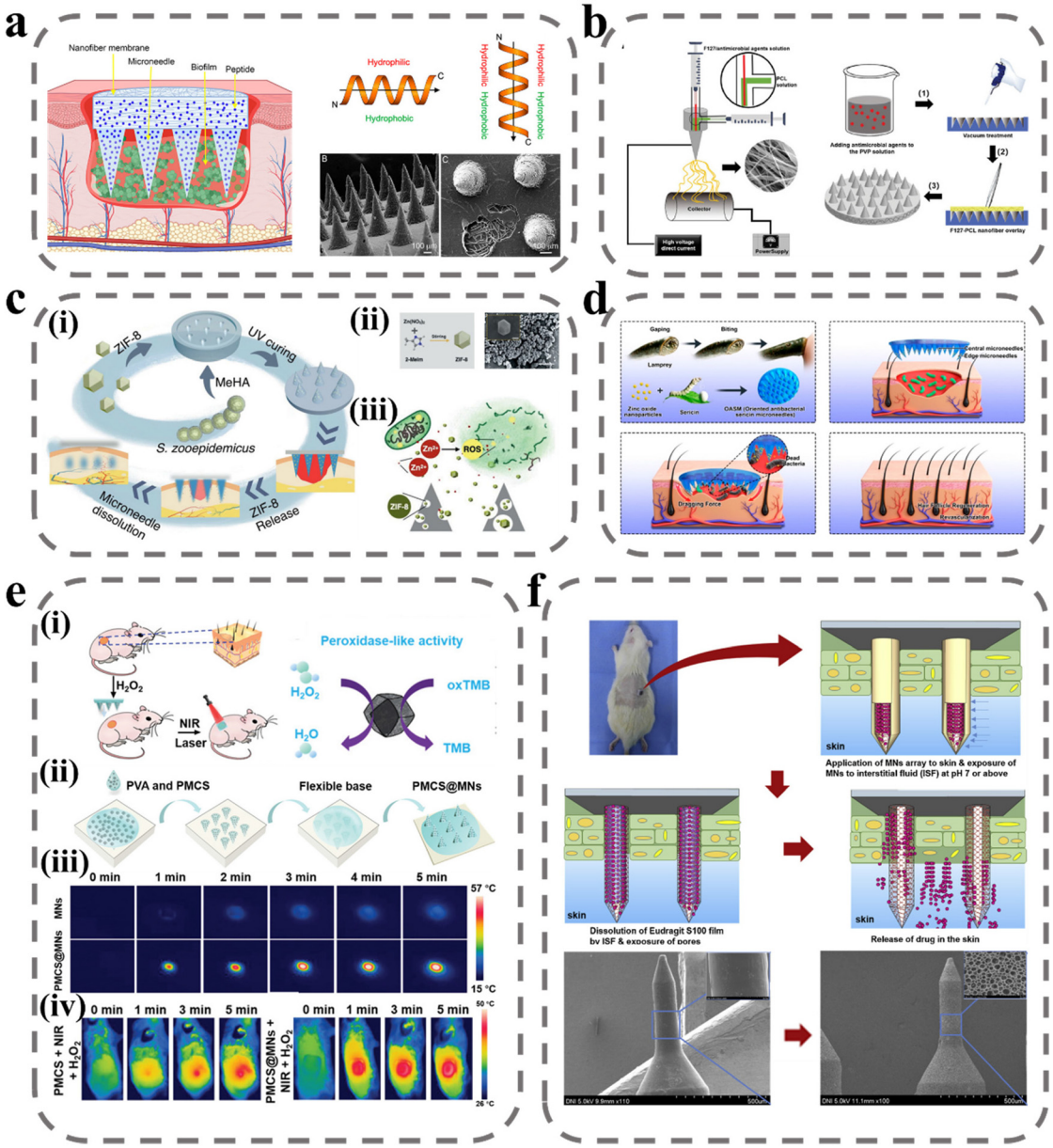

Fig. 3 MNs for wound antibacterial effects. (a) Schematic illustrating Janus-type antimicrobial dressings consisting of molecularly engineered peptide-loaded electrospun nanofiber membranes and microneedle arrays for the treatment of biofilms in chronic wounds.[96] Reprinted from the American Chemical Society, Copyright 2020. (b) Schematic illustrating the fabrication of biphasic scaffolds.[97] Reprinted from John Wiley and Sons, Copyright 2021. (c) Zn-MOF encapsulated antibacterial and degradable microneedles array for promoting wound healing:[99] (i) schematic illustration of the fabrication and application of the MeHA/ZIF-8 MNs; (ii) schematic diagram of ZIF-8 synthesis process and SEM images of ZIF-8 nanoparticles; (iii) schematic of the antibacterial effect of ZIF-8 nanoparticles. Reprinted from John Wiley and Sons, Copyright 2021. (d) Design and fabrication of bioinspired oriented antibacterial sericin MNs for infected wound healing.[100] The microneedles consist of silk glue and zinc oxide nanoparticles (ZNPs) that degrade and release ZNPs into the wound to kill bacteria, and the marginal needles provide dragging force to stimulate wound contraction. Reprinted from the American Chemical Society, Copyright 2022. (e) NIR laser-triggered microneedle-based liquid band-aid for wound care:[101] schematic illustrating the (i) mechanism and (ii) fabrication of NIR laser-triggered MNs; (iii) real-time infrared thermal images of MNs and PMCS@MNs. (iv) The infrared thermal images of mice with various treatments. Reprinted from John Wiley and Sons, Copyright 2021. (f) Wound pH-dependent release system schematic illustration.[102] Reprinted from Elsevier, Copyright 2021.

the catalytic effect of the ZIF-8 suspension on ROS was verified. Deng *et al.* designed a variety of targeted antimicrobial filamentous MNs with targeted traction, debridement, and wound-repair enhancement inspired by the teeth of the seven-gill eel.[100] As shown in Fig. 3d, the needles on the circular part of the MNs have been tucked in at an angle of 30° to the center, which provides traction for wound closure at the wound site. In addition, the body of the MNs was loaded with active zinc oxide nanoparticles to ensure antibacterial activity. In antimicrobial testing in the mouse model, the CFU count of

 This journal is © The Royal Society of Chemistry 2023

Published on 03 mai 2023. Downloaded on 05.06.2026 15:09:01.

S. aureus was reduced from 10.4×10^6 to 0.04×10^6. In order to improve the controllability of the treatment process, Sun *et al.* introduced photoinitiated technology into the MNs system. PVA was used as a substrate for solubilizing MNs and loaded with MOF-derived multifunctional porphyrin-like metal-centered nanoparticles for photothermal conversion and nano enzyme activity.[101] As shown in Fig. 3e, the porphyrin-like metal-centered nanoparticles can convert light energy into heat energy to accelerate the dissolution of PVA and enhance drug penetration under NIR excitation, and can catalyze hydrogen peroxide to generate ROS to disrupt the membrane structure of bacteria to achieve controlled bactericidal activity.

Although the above treatments are highly sterilizing, they are equally toxic to the normal tissues at the wound site. To precisely and selectively deliver antimicrobial drugs to the site of action and avoid the undesirable side effects of high doses, intelligent drug release can be achieved using dynamic changes in the microenvironment of the upper bacterial biofilm, including pH, specific bacterial enzymes, higher temperature, *etc*. Ullah *et al.* took advantage of the alkaline environment at the wound site by capping the surface of porous MNs with a film of Eudragit S100, a pH-sensitive material that dissolves in the alkaline pH environment of the wound and releases the drug loaded in the porous MNs into the biofilm to achieve responsive therapy.[102] In addition, enzymes in bacterial biofilms can also be used for the smart administration of drugs. Mir *et al.* prepared bacterial lipase-sensitive poly(ε-caprolactone) polymers in nanoparticles loaded with carvacrol to achieve a specific release of drugs using bacterial lipase.[103] Lei *et al.* coupled the antimicrobial photothermal peptide AMP-Cypate to gelatin nanoparticles to achieve responsive release based on gelatinase secreted by *S. aureus* and kill pathogens by near-infrared-excited photothermal conversion (Table 1).[104]

2.3 Microneedles for proliferation

The proliferative phase of wound healing is a complex and critical stage that involves a multitude of signaling molecules and immune cells. It is characterized by angiogenesis, granulation tissue formation, and re-epithelialization, which are essential processes for successful wound healing.[107] In particular, the formation of blood vessels is crucial as it provides oxygen, nutrients, and immunomodulatory signal messengers for cell proliferation in the wound site. To promote vascular regeneration, pro-vascular regeneration therapy involves the delivery of vascular endothelial growth factor (VEGF), nitric oxide (NO), and other signaling molecules. However, in the proliferative phase, a shift from the inflammatory phase to the anti-inflammatory phase occurs, and interference from factors such as bacterial infection and diabetes can prolong the inflammatory state, hindering the effects of pro-wound healing signaling factors.[46,108,109] Therefore, human intervention is necessary to regulate the immune and promote the transformation of immune cells from a pro-inflammatory to an anti-inflammatory repair type and reduce the high ROS environment in the inflammatory phase. The current promotion of value-added wound repair is mainly oriented to two aspects; one is to regulate inflammation and the other is to promote proliferative repair.

Oxygen is a fundamental element necessary for life and critical for successful wound healing, as it promotes cell proliferation and tissue remodeling. To address this, Zhang *et al.* developed an MN system loaded with oxygen-rich hemoglobin doped with black phosphorus (BP) for photothermal conversion (Fig. 4a).[110] The BP was shown to increase the temperature of the wound site upon exposure to near-infrared light, leading to the release of oxygen from hemoglobin. *In vitro* testing demonstrated effective control of oxygen release, and programmed oxygen release was achieved *via* indirect exposure to NIR. In animal experiments, wounds healed almost completely within just 9 days. To promote the migration and proliferation of endothelial fibroblasts at the wound site, Zhang *et al.* applied electrical stimulation by MNs at the wound site to simulate endogenous wound-healing mechanisms to guide cell migration and enhance cell metabolism, proliferation, and differentiation to promote wound healing.[111] They introduced liquid metal into the MN system as a conductive layer and improved the adhesion of MNs by mimicking the structure of an eagle's claw. In *in vitro* experiments, NIH 3T3 cells were stimulated by electric fields with greatly increased proliferation capacity accompanied by electrical signal movement without causing cell damage (Fig. 4b). To repair the skin damage caused by the tumor photothermal treatment process, Shan *et al.* used sodium alginate/gelatin/hyaluronic acid as a support layer for MNs.[112] The sodium alginate/gelatin/hyaluronic acid support layer covering the wound promoted the proliferation of endothelial cells and fibroblasts, which in turn enhanced skin regeneration (Fig. 4c). In animal skin-repair experiments, rats in the MNs administration group had complete regeneration of skin tissue with skin appendages and increased cell density, indicating an accelerated rate of skin repair.

In diabetic patients, high glucose conditions inhibit angiogenesis and restrict the transport and delivery of nutrients and oxygen in diabetic wounds. To stimulate vascular regeneration at the wound site, Guan *et al.* delivered VEGF *via* MNs to the wound site. As shown in Fig. 4d, VEGF and Prussian blue nano enzymes were encapsulated in SilMA to prepare MN bodies that were slowly released after puncture into the subcutis.[113] Prussian blue nano enzymes exert their therapeutic effects by scavenging reactive oxygen species and inhibiting inflammation. VEGF is a multifunctional cytokine that plays a major role in stimulating angiogenesis by binding to endothelial cell receptors. In an *in vitro* test, the MNs group exhibited HUVEC tube-forming ability. After diabetic wound treatment, angiogenesis in animals was assessed by anti-CD31 and anti-α-SMA immunofluorescent stains, with higher vascular density in the MN-treated group. NO gas acts as an important pro-angiogenic cell signaling agent for endothelial cells. Yao *et al.* designed a novel porous metal–organic framework MN array patch to achieve controlled release of NO.[114] The authors prepared HKUST-1 by a multi-step hydrothermal high-pressure method and covered its surface with a monolayer of GO, which was

Published on 03 mai 2023. Downloaded on 05.06.2026 15:09:01.

Table 1 Summary of MN-based systems for wound antibacterial

MNs materials	Drugs	Mechanism	Models	Ref.
HA	Green Tea	Catechins disrupt cell membranes and break down essential metabolites	*In vitro*: Luria–Bertani medium *In vivo*: Sprague–Dawley rats' wounds Strains: *E. coli*; *S. typhimurium*; *P. putida*; *B. subtilis*; *S. aureus*	91
Gantrez AN-139	Methylene Blue	Destruction of bacteria by the photoinitiated generation of highly reactive free radicals	*In vitro*: Mueller-Hinton Broth; Sabouraud Dextrose Broth Strains: *E. coli*; *S. aureus*; *C. albicans*	105
Manuka honey	Methylglyoxal	Anti-biofilm activity	*In vitro*: blood agar culture dish Strains: MRSA	92
PVA/PVP	Carvacrol-PCL nanoparticles	Bacterial lipase responds to the degradation of PCL to release Carvacrol	*In vitro*: Mueller–Hinton Broth; Luria–Bertani Broth *In vitro*: *ex vivo* pig skin Strains: *S. aureus*; *P. aeruginosa*	103
F127/PCL PVP	AMP-W379	PVP releases the drug rapidly by dissolution and the fibrous scaffold releases the antimicrobial peptide slowly	*In vitro*: Tryptic Soy Broth *In vitro*: *ex vivo* human skin tissue *In vivo*: mouse wounds *In vivo*: human wounds Strains: MRSA; *K. pneumoniae*; *A. baumannii*; *P. aeruginosa*	96
HA/PVP	Azithromycin	Inhibits bacterial protein synthesis to produce bacterial inhibition	*In vitro*: Agar medium *In vivo*: male albino rats' wounds Strains: *E. coli*; *S. enterica*; *S. aureus*	90
F127/PCL PVP	$AgNO_3$, $Ga(NO_3)_3$, and vancomycin	PVP releases the drug rapidly by dissolution and the fibrous scaffold releases the drugs slowly	*In vitro*: *ex vivo* human skin tissue *In vivo*: human wounds Strains: MRSA; *P. aeruginosa*	97
PVA	Porphyrin-like metal centers nanoparticles	Under near-infrared excitation, it converts light energy into heat energy, accelerates the dissolution of PVA, enhances drug penetration, and catalyzes the production of ROS from hydrogen peroxide	*In vitro*: beef extract peptone medium *In vivo*: BALB/c male mice wounds Strains: *S. aureus*	101
PLGA/Eudragit S100		By pH response, Eudragit S100 dissolves and releases the drug in a high pH environment		102
MeHA	ZIF-8	Zn^{2+} can cell wall direct contact, leading to disruption of bacterial cell integrity, in addition to catalyzing the production of ROS	*In vitro*: PBS *In vivo*: Sprague–Dawley rats' wounds Strains: *S. aureus*; *E. coli*	99
Sericin	Zinc oxide nanoparticles	Zn^{2+} can directly contact cell wall, leading to disruption of bacterial cell integrity, in addition to catalyzing the production of ROS	*In vitro*: Luria–Bertani medium *In vivo*: mice wounds Strains: *S. aureus*; *E. coli*	100
Recombinant Human Collagen III/PVP	AMP-Cypate/gelatin nanoparticles	Responsive release based on gelatinase secreted by *S. aureus* and killing of pathogens by near-infrared-excited photothermal conversion	*In vitro*: Luria–Bertani medium *In vivo*: Diabetic rats' wounds Strains: *S. aureus*	104
CS/TA	Ag nanoparticles	Inhibiting bacterial division by binding to the bacterial membrane proteins responsible for transport as well as DNA Interferes with bacterial cellular respiration and disrupts energy production	*In vitro*: Luria–Bertani medium *In vitro*: anti-biofilm *in vitro* model *In vivo*: Sprague–Dawley rats' wounds Strains: *S. aureus*; *E. coli*; MRSA	106
Chitosan/Fucoidan	Kangfuxin		*In vitro*: Luria–Bertani and Tryptic Soy Broth Strains: *S. aureus*; *E. coli*	93

This journal is © The Royal Society of Chemistry 2023

Published on 03 mai 2023. Downloaded on 05.06.2026 15:09:01.

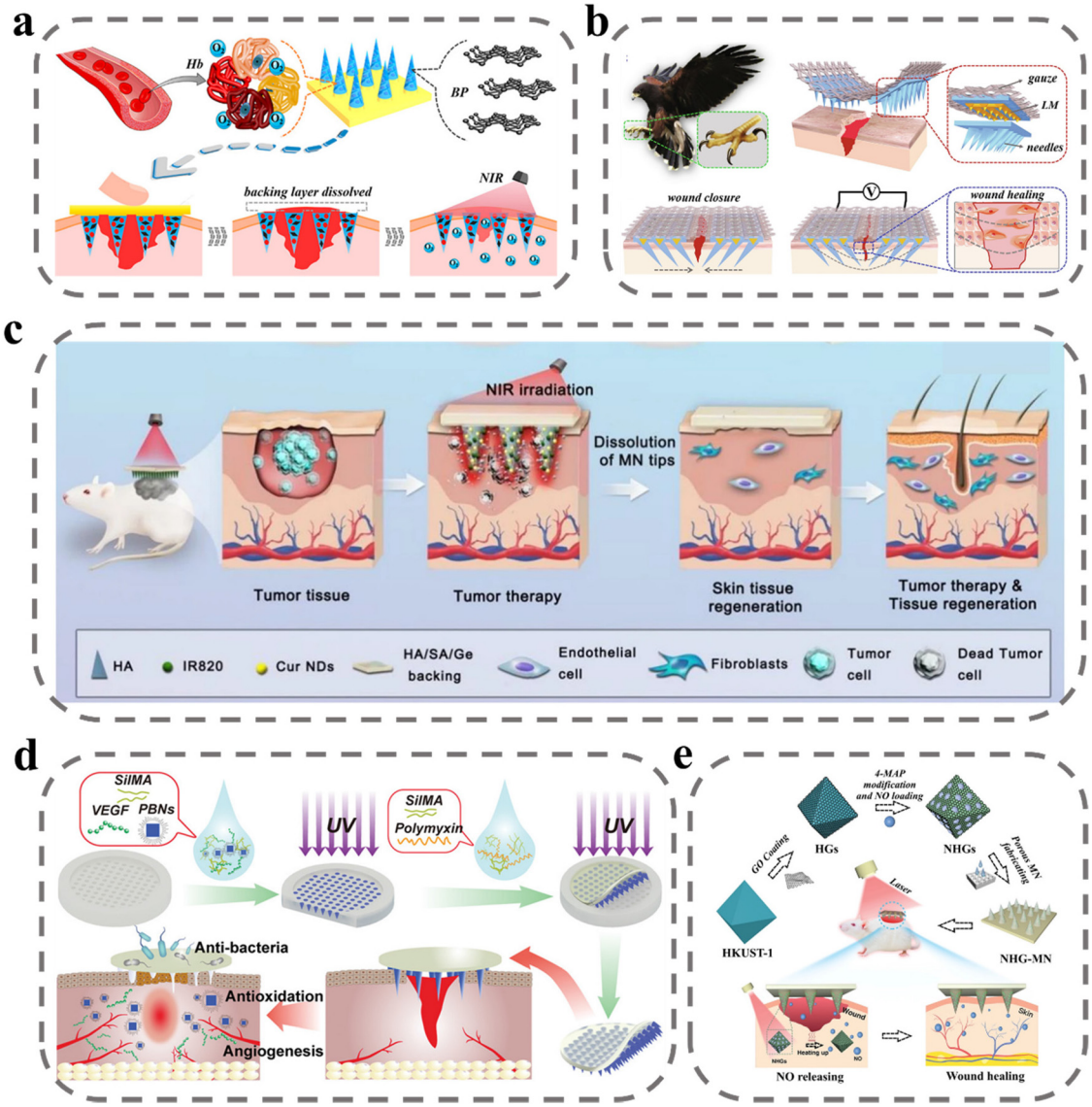

Fig. 4 MNs for wound proliferation. (a) Schematic illustrations of wound healing using NIR-responsive separable MNs which encapsulate BP QDs and oxygen-carrying Hb.[110] Reprinted from the American Chemical Society, Copyright 2020. (b) Schematic illustration of the claw-inspired microneedle patch with liquid metal encapsulation and its wound-healing application.[111] The structure, composition and application of the microneedle patch, which could tighten the wound area and prevent dehiscence by connection to the external power source. Reprinted from Elsevier, Copyright 2021. (c) Schematic illustration of Cur NDs/IR820/HA MN for tumor chemo-photothermal therapy and skin tissue regeneration.[112] Reprinted from Springer Nature, Copyright 2022. (d) Schematic presentation of the fabrication and application of MN-PBNs-VEGF patches for promoting diabetic wound healing.[113] Reprinted from John Wiley and Sons, Copyright 2022. (e) Schematic diagram of the preparation and application of the porous MOF MN array, which was fabricated by PEGDA and encapsulated with NHGs *via* a template infusion method.[114] Reprinted from John Wiley and Sons, Copyright 2022.

subsequently modified on its surface by 4-MAP through the formation of *N*-diazadioate moieties for NO adsorption. Controlled release of NO was achieved under NIR by the photothermal conversion of GO to generate heat. In animal experiments, it was evident that under the stimulation of NO, there was significant vascular regeneration at the wound site, and this promoted wound healing (Fig. 4e).

In diabetic wounds, persistent inflammation and high ROS are important factors that hinder the transition to the proliferative phase of wound repair. The main therapeutic idea for this is to modulate the immune system to reduce inflammation and lower ROS levels. There have been some MN studies to reduce the inflammatory response at the wound site by delivering anti-inflammatory drugs, immune signaling molecules, *etc.*, and to reduce ROS levels using biomaterials such as gallnut and PDA.[109,115–118] And there has been noteworthy research in recent years based on MN technology to deliver cells and exosomes to achieve cell therapy. MSC-derived

Published on 03 mai 2023. Downloaded on 05.06.2026 15:09:01.

exosomes are nanoscale extracellular vesicles with complex components such as proteins, lipids, and nucleic acids that enable complex immunotherapies and exhibit superior capabilities in tissue repair and regeneration, with high stability, easy storage, and low immunogenicity. As shown in Fig. 5a, Gan *et al.* loaded MSC-exos into porous GelMA hydrogels to continuously deliver anti-inflammatory and pro-angiogenic MSC-exos to wounds to improve cellular function, remodel blood vessels and restore the immune system to accelerate healing.[119] In *in vitro* cellular assays, MSC-exos promoted HUVEC migration, angiogenesis and induced macrophage transition from M1 to M2 phenotype. However, high levels of ROS at the wound site were detrimental to achieving functional expression of exosomes. To overcome the detrimental effects of ROS-derived oxidative stress, Ma *et al.* proposed a novel core–shell hyaluronic acid MNs patch.[120] PDA nanoparticles were encapsulated in a shell with HAMA, and with the lysis and degradation of HAMA, PDA nanoparticles were slowly released to reduce ROS levels to suppress inflammation. Ferrum-mesenchymal stem cell-derived artificial nanovesicles were mixed with HA solution to prepare nuclei for MNs; after the degradation of the HAMA shell to reduce ROS levels, nanovesicles were released to regulate immunity, promote M2 macrophage polarization, further inhibit wound inflammation, and accelerate angiogenesis, cell migration, and proliferation (Fig. 5b). Stem cells can produce various bioactive substances to repair the function of tissues and organs. Besides secreting growth factors to promote angiogenesis and extracellular matrix reconstruction, they can also produce cytokines to exert immunomodulatory effects. Xu *et al.* loaded human adipose stem cells into MNs prepared using HAMA and doped them with platelet-derived growth factor D (PDGF-D).[46] PDGF-D is believed to play an important role in ADSC proliferation, differentiation, and migration, which can enhance the cellular function of ADSC and further promote wound healing (Fig. 5c). In the cell viability test, cell viability

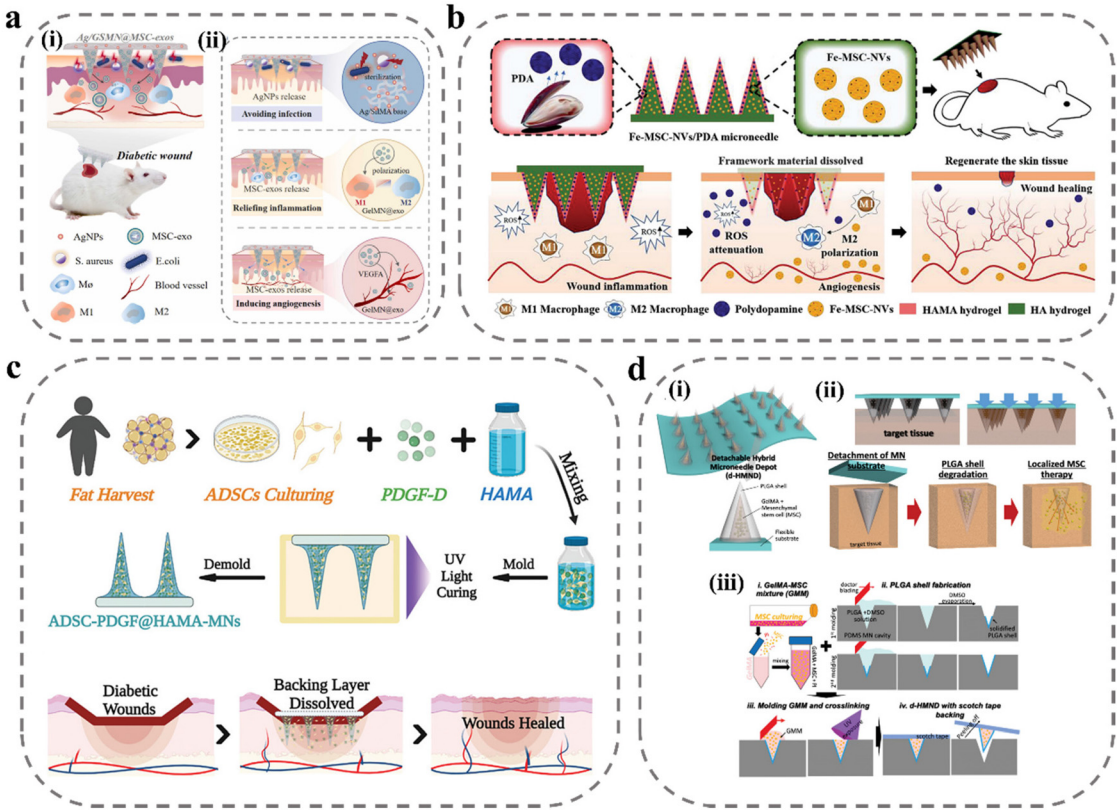

Fig. 5 MNs for delivery of exosomes and stem cells. (a) Illustration of the MSC-exos-loaded MN patch for promoting wound healing:[119] (i) after insertion, the supporting base adhered to the skin wound site to kill bacteria, and the MN tips were implanted into a deeper layer of the wound, allowing for sustained release of the MSC-exos; (ii) the healing mechanisms of the MN system: AgNPs incorporated into MN patches were capable of inhibiting microbial pathogen growth at the wound surface; MSC-exos were transported into the dermis through the needle tips, which can inhibit chronic wound-associated inflammation by macrophages polarization, and induce the growth of blood vessels *via* VEGFA. Reprinted from Elsevier, Copyright 2022. (b) Schematic illustrations of Fe-MSC-NVs/PDA MN patch for diabetic wound healing.[120] Reprinted from John Wiley and Sons, Copyright 2022. (c) Schematic illustrations of the MN system loaded with ADSCs and PDGF-D for diabetic wound treatment.[46] Reprinted from John Wiley and Sons, Copyright 2022. (d) Schematic illustrations of detachable hybrid MN depot (d-HMND) for localized delivery of mesenchymal stem cells:[108] (i) an assembled d-HMND consisting of an array of MNs with PLGA shells, filled with a GelMA-MSC mixture, and fixed to a flexible substrate; (ii) the working mechanism of the MNs delivered by the d-HMND after application to target tissue; (iii) sequential fabrication of a d-HMND. Reprinted from John Wiley and Sons, Copyright 2020.

 This journal is © The Royal Society of Chemistry 2023

Published on 03 mai 2023. Downloaded on 05.06.2026 15:09:01.

Table 2 Summary of MN-based systems for proliferation

Materials	Specification (μm)	Drug carriers	Drugs	Mechanism	Ref.
Biomass Chitosan	20 × 20, height 600, base diameter 300	*N*-Isopropyl acrylamide	VEGF	Drug release in response to changes in wound temperature	121
PVP/GelMA			Black phosphorus/ oxygen-carrying hemoglobin	In the NIR, BP QDs can rapidly convert light energy into heat, thus increasing the local temperature and thus reducing the oxygen binding capacity of Hb, leading to controlled oxygen transport	110
PLGA/GelMA	8 × 8, height 700, base diameter 450, spacing 1850		MSCs	PLGA shell degradation and MSCs secrete anti-inflammatory repair markers in GelMA gels to promote healing	108
PP	Claw, height 750–800, base diameter 400			Electrical stimulation can direct cell migration to enhance cell metabolism, proliferation, and differentiation	111
3-(Acrylamide) PBA-doped PEGDA			Mxene/Adenosine	Under NIR irradiation, MXene rapidly converts light into heat, which accelerates the release of loaded adenosine and activates G protein-coupled adenosine receptors to regulate cellular behavior to maintain activation signals around the site of injury	122
PEGDA	15 × 15, height 600, base diameter 300		Little Leaf Cypress/ Centella Asiatica	Promotes the expression of relevant growth factor genes in fibroblasts, as well as antioxidant and anti-inflammatory	115
SF	Height 1000, base diameter 270, spacing 600	*N*-Isopropyl acrylamide	VEGF/Mupirocin	Drug release in response to changes in wound temperature with an inverse opal photonic crystal structure to improve drug loading	123
PEGDA	15 × 15	GO-wrapped MOF	NO	Light responds to photothermal conversion to release NO, which stimulates vasodilation and angiogenesis, signaling and integration, elimination of infection, and immune regulation	114
γ-PGA	10 × 10, height 500, base diameter 200	Mg-MOF	Gallic acid	The released Mg^{2+} induces cell migration and tubulogenesis, while gallic acid is a reactive oxygen scavenger that promotes antioxidation	109
HA	10 × 10, height 600, base diameter 300, spacing 600	PLGA nanoparticles	Naproxen/rhCol III	rhCol III increases cell adhesion, PLGA releases naproxen anti-inflammatory	124
AlgMA	20 × 20, height 600, base diameter 250, spacing 550		Trichostatin A/ $HDAC_4$	TSA demonstrated the ability to inhibit NLRP3 inflammatory vesicle activation, reduce the risk of NLRP3-mediated macrophage focal death, and promote macrophage phenotypic polarization. $HDAC_4$ is involved in inflammatory regulation reducing IL-1β secretion and IL-10 expression promoting M2	118
CS/PVP			Panax notoginseng saponin/Mg	Regulates macrophage phenotype, inhibits membranous granulocyte inflammation and promotes the transition from the inflammatory phase to the tissue repair and tissue remodeling phase in chronic wounds	117
MeHA	10 × 10, height 600, base diameter 300		CINP@SiO_2	SiO^{4-}_4 inhibits oxidative stress and inflammatory responses in macrophages promoting endothelial cell proliferation and angiogenesis and accelerates recovery of all dermal defects and infected wounds	116
HAMA/HA	20 × 20, height 860, base diameter 360, spacing 700		PDA NPs/Fe-MSC-NVs	PDA NPs were consistently released at the lesion to suppress ROS-induced inflammatory responses, whereas Fe-MSC-NVs significantly increased HUVEC migration, proliferation, and tube formation. The combination of PDA NPs and Fe-MSC-NVs further promoted M2 macrophage polarization	120
GelMA/PEGEDA	16 × 16, height 600, base diameter 300	β-CD-AOI_2	Tazarotene/exosomes	Tazarotene is a retinoid that effectively promotes angiogenesis, hair follicle, and collagen regeneration in wound repair. Externally, exosomes transfer the bioactive cargo contained (including miRNA, mRNA, and proteins) to regulate communication between cells	125
SA/Ge/HA	20 × 20, height 540, spacing 700		SA/Ge/HA	SA/Ge/HA backing layer stimulates the regeneration of skin tissue and promotes the proliferation of endothelial cells and fibroblasts	112

Published on 03 mai 2023. Downloaded on 05.06.2026 15:09:01.

Table 2 *(Contd.)*

Materials	Specification (μm)	Drug carriers	Drugs	Mechanism	Ref.
PCL/gelatin	Height 800, base diameter 350, spacing 650		PDA/CaO_2/metformin	Provides O_2 lowers reactive oxygen levels, lowers blood glucose levels at the wound site, and thus improves vascular regeneration	126
HAMA	15 × 15, height 800, base diameter 500		PDGF-D/ADSCs	ADSC not only secrete growth factors to promote angiogenesis and extracellular matrix reconstruction but also produce cytokines to exert immunomodulatory effects. PDGF-D is thought to play an important role in ADSC proliferation, differentiation, and migration, enhancing the cellular function of ADSC	46
SFMA	Height 700, spacing 700		Prussian blue nano enzyme/VEGF	Scavenging reactive oxygen species and inhibiting inflammation to exert its therapeutic effects, VEGF is a multifunctional cytokine that plays a major role in stimulating angiogenesis by binding to endothelial cell receptors	113
GelMA/SilMA	Height 600, base diameter 450, spacing 650		MSC-exos	Accelerates healing by improving cellular function, remodeling blood vessels, and restoring the immune system	119
Polylysine/gelatin			NO	The specific transamination reaction of glutamine aminotransferase and soluble microneedle patches enables the deep release of NO gas under physiological conditions	127

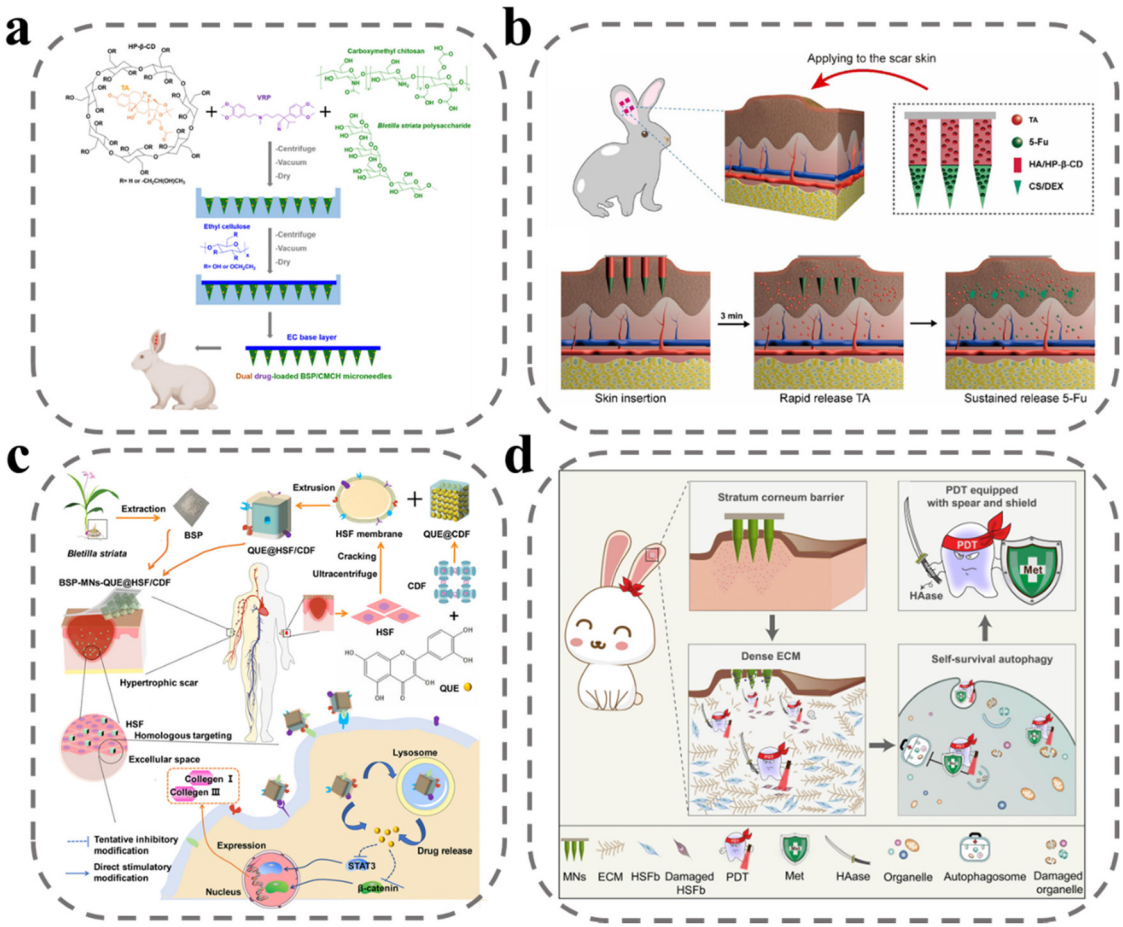

Fig. 6 MNs for anti-scar. (a) An illustration of an MN patch preparation and its application for co-delivery of triamcinolone acetonide and verapamil.[130] Reprinted from Elsevier, Copyright 2022. (b) Schematic illustration of HS model in rabbit ear, the design of the BMN with 5-Fu in the tip layer and TA in the tail layer of the needle.[131] Reprinted from Elsevier, Copyright 2021. (c) Schematic illustration of fabrication and administration of BSP-MNs-QUE@HSF/CDF.[132] Reprinted from the American Chemical Society, Copyright 2021. (d) Schematic illustration of MNs with combination treatment of 5-aminolevulinic acid-mediated photodynamic therapy, hyaluronidase, and metformin.[133] Reprinted from Elsevier, Copyright 2022.

This journal is © The Royal Society of Chemistry 2023

Published on 03 mai 2023. Downloaded on 05.06.2026 15:09:01.

could be maintained at 90% within 24 hours and stable VEGF secretion could be detected. However, in MNs prepared from hydrogels it is difficult to reconcile the relationship between mechanical properties and cellular activity. To ensure cell viability, the degree of cross-linking of hydrogel MNs is limited and the drying process cannot be performed, and the mechanical properties are often difficult to achieve. As shown in Fig. 5d, to solve this problem, Lee *et al.* designed MNs with a core–shell structure for local delivery of MSCs in regenerative therapy.[108] MSCs were mixed with GelMA solution to form the core of the MNs and PLGA to form the shell of the MNs to ensure the penetration ability of the MNs. This core–shell structure greatly improves the mechanical properties of the MNs while ensuring cell viability. In the MN system, MSCs did not lose their cellular functions and could stably secrete VEGF, showing a higher wound-closure rate, improved re-epithelialization, and a richer vascular system in wound-recovery assays (Table 2).

2.4 Anti-scarring microneedles

Scar, a pathological tissue characterized by the excessive deposition of collagen by fibroblasts, is a result of severe infections and abnormal inflammatory responses during the wound-healing process.[128] There is no clear evidence that scars pose a potentially significant risk to the human body, but the main effects are pruritus, skin stiffness, and the potential for psychological trauma and social problems due to aesthetic discomfort. Currently, the main treatment options for scars include surgery, laser therapy, radiation therapy, and medication.[129] Among these, pharmacological treatment is the most convenient, as it reduces fibroblast activity and down-regulates collagen expression. However, the efficacy of drug therapy is limited by poor drug delivery and potential side effects. To address this challenge, MNs offer a promising solution by facilitating efficient drug delivery through the creation of micro-channels within the skin with minimal discomfort

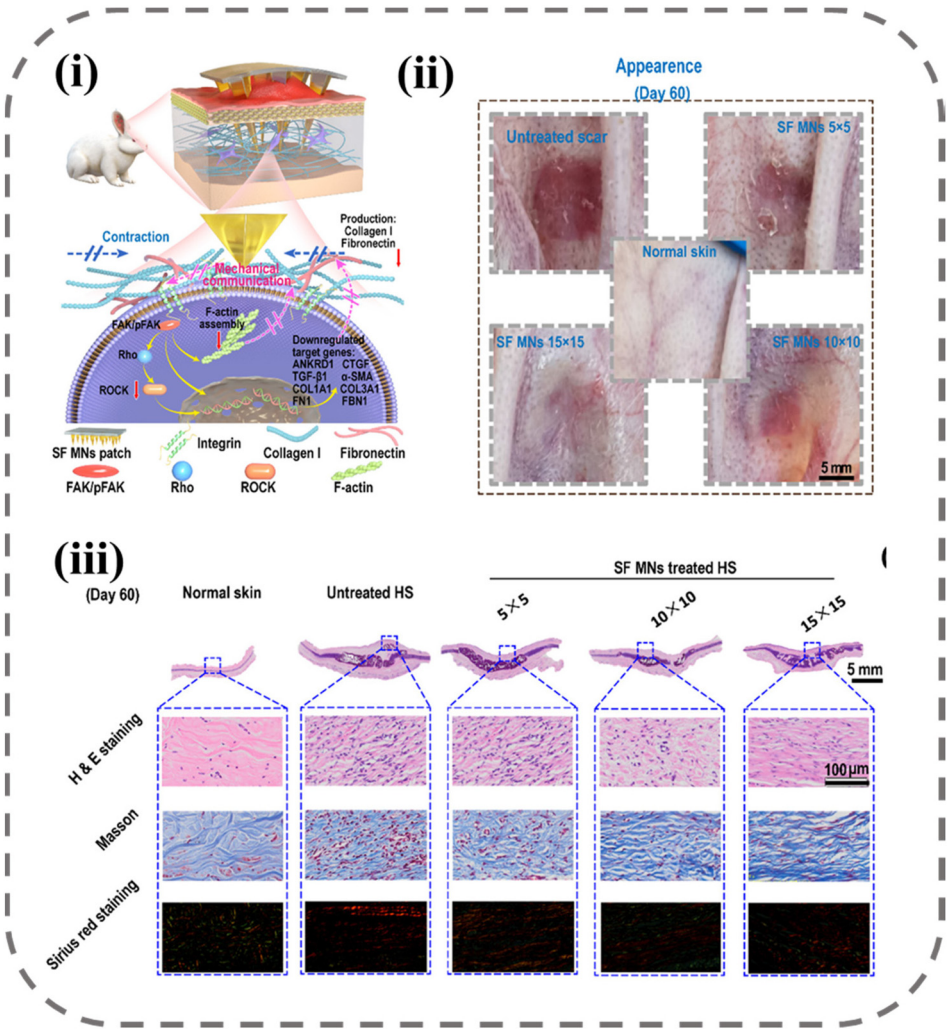

Fig. 7 Down-regulating scar formation by MNs directly *via* a mechanical communication pathway:[134] (i) illustration of SF MN interrupting the mechanical communication between fibroblasts and the ECM to prevent fibroblast activation and promoting ECM remodeling with reduced secretions of collagen I and fibronectin *via* the integrin-FAK signaling pathway; (ii) appearances of post-treated scar tissues; (iii) representative H&E, Masson, and Sirius red staining images of scar tissue and normal skin sections. Reprinted from the American Chemical Society, Copyright 2022.

Published on 03 mai 2023. Downloaded on 05.06.2026 15:09:01.

and high drug efficacy with low dosages, reducing the likelihood of side effects.

Three main categories of drugs have been utilized for the treatment of scars, including glucocorticoids such as dexamethasone and triamcinolone acetonide, anticancer drugs such as 5-fluorouracil, and calcium channel inhibitors such as verapamil. Previous studies have demonstrated the successful loading of these drugs into MNs, resulting in improved therapeutic outcomes. In a study by Zhang *et al.*, triamcinolone acetonide and verapamil were co-loaded into MN sites to achieve a synergistic treatment effect (Fig. 6a).[130] Hydroxypropyl β-cyclodextrin was utilized to encapsulate tretinoin, increasing the loading of the non-water-soluble drug and improving its efficacy. Treatment with this method resulted in reduced thickness of scars, decreased expression of hydroxyproline and TGF-β1 in scars, improved collagen fiber alignment, and reduced dermal congestion and hyperplasia. Yang *et al.* developed an MN with dual solubilization properties, with the tip site composed of chitosan and dextran for the slow release of 5-fluorouracil, and the second half of the needle body prepared from HA and treated with hydroxypropyl-β cyclodextrin wrapped with insoluble tretinoin for rapid release of triamcinolone acetonide (Fig. 6b).[131] Administration of this MN treatment led to decreased expression of both Col I and TGF-β1-related mRNA and protein.

Hydrophobic drugs such as quercetin have been shown to be effective in downregulating fibroblasts and collagen. However, its non-water solubility makes it difficult to load into microneedles, and it becomes a challenge to improve the subcutaneous accumulation and bioavailability of the drug. To address this challenge, Wu *et al.* developed a diphenyl carbonate cross-linked cyclodextrin metal–organic backbone that could effectively load quercetin to increase subcutaneous accumulation (Fig. 6c).[132] Cell membrane-mediated active targeting delivery systems have been demonstrated as a promising approach for improving clinical efficacy. In this study, the researchers utilized scar fibroblast cell membranes to wrap the diphenyl carbonate cross-linked cyclodextrin metal–organic backbone, allowing for targeted delivery to homologous cells to improve bioavailability of drug. An *in vitro* analysis showed that coumarin 6-labeled metal–organic skeletons wrapped in cell membranes displayed higher fluorescence response in human embryonic skin fibroblasts compared with metal–organic skeletons without cell membrane wrapping. Huang *et al.* loaded hyaluronidase, metformin, and 5-aminolevulinic acid onto MNs to achieve a "three birds with one stone" effect (Fig. 6d).[133] Hyaluronidase, a specific degradation enzyme of HA, was employed to enhance drug diffusion, as HA is the main component of the extracellular matrix that binds tightly to collagen fibers and hinders drug diffusion. Metformin was

Table 3 Summary of MNs-based systems for anti-scar

Materials	Specification (μm)	Drug carriers	Drugs	Mechanism	Ref.
HA	125 needles, height 1200, base diameter 300, spacing 900	Hydroxypropyl-β-cyclodextrin	Triamcinolone acetonide	Inhibits fibroblast proliferation and collagen synthesis, increases collagenase production and reduces collagenase inhibitors	135
HA	10 × 10, height 1000, base diameter 300		Shikonin	Inhibits cell viability, cell proliferation, and collagen production in scar-derived fibroblasts	136
Stainless steel	Length 700, width 160, thickness 75	Carboxymethyl chitosan nanoparticles	5-Fluorouracil	Inhibition of thymidine synthase, which is associated with the conversion of uridine to thymidine, which inhibits the synthesis of deoxyribonucleic acid	137
PVP/BSP	10 × 10, height 380, base diameter 230, spacing 480	Diphenyl carbonate cross-linked cyclodextrin metal–organic skeleton	Quercetin		132
CS/DEX/HA	12 × 12, height 1200, base diameter 300, spacing 800	Hydroxypropyl-β-cyclodextrin	Triamcinolone acetonide, 5-fluorouracil		131
SF	5 × 5, 10 × 10, 15 × 15, height 1000, base diameter 300			Induced mechanical communication between fibroblasts and ECM is blocked and mechanical stress generated by fibroblasts is reduced	134
PEG/PVP/PVA		Pluronic F127 nanomicelles	Trinostat	Inhibits the release of inflammatory cytokines from monocytes and macrophages and has an anti-fibrotic effect by inhibiting the formation and accumulation of collagen	138
HA	Height 600, base diameter 300, spacing 500	Tyramine-modified gelatin	siSPARC	Down-regulation of SPARC and Col1a1 genes reduces collagen deposition	139
PVP			5-Aminolevulinic acid, hyaluronidase, metformin	Under laser irradiation, ALA is converted to PpIX and produces ROS to kill fibroblasts; Met interferes with the cellular autophagy process to cause cell death	133
CMCH/BSP/EC	Height 800	Hydroxypropyl-β-cyclodextrin	Triamcinolone acetonide, verapamy	Verapamy: calcium channel inhibitors	130

 This journal is © The Royal Society of Chemistry 2023

Published on 03 mai 2023. Downloaded on 05.06.2026 15:09:01.

also utilized, as it has been shown to interfere with cellular autophagy and participate in photodynamic therapy. According to the mechanism of 5-aminolevulinic acid-mediated photodynamic therapy, the conversion of 5-aminolevulinic acid to PpIX under laser irradiation generates large amounts of ROS to produce cytotoxicity to kill fibroblasts. The combination treatment of 5-aminolevulinic acid-mediated photodynamic therapy, hyaluronidase, and metformin was found to have excellent therapeutic effects, with the lowest scar elevation index, downregulation of collagen I and TGF-β1 expression, and reduction of LC3 II/I ratio observed in pharmacodynamic studies.

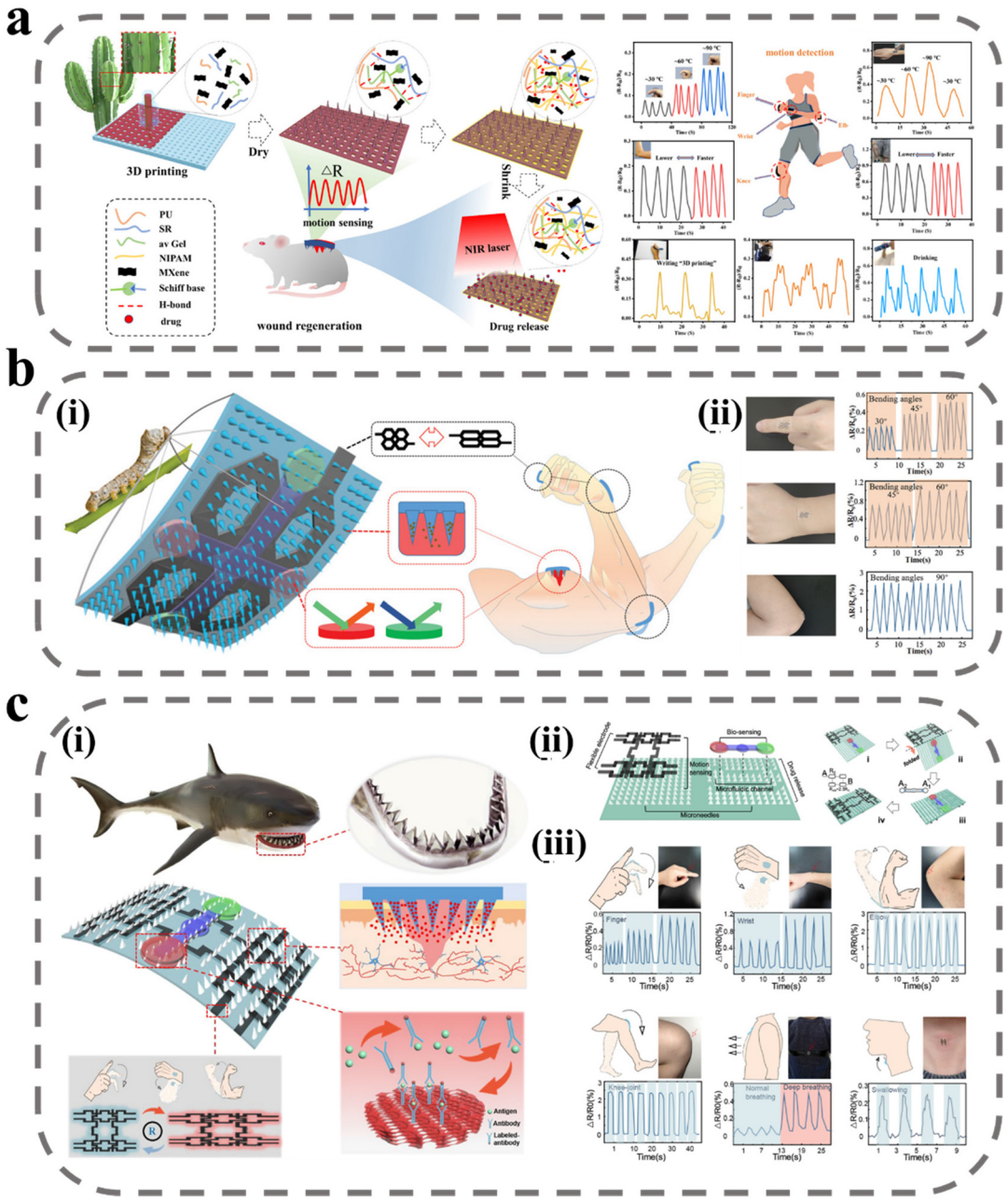

Fig. 8 MNs for wound monitoring. (a) Schematic illustration of 3D-printed bionic near-infrared light-responsive MXene and spidroin-based microneedle scaffolds for skin wound healing.[149] Reprinted from the American Chemical Society, Copyright 2022. (b) Intelligent silk fibroin-based microneedle dressing:[150] (i) schematic diagram of intelligent, biocompatible, stretchable, and highly integrated i-SMD for biochemical sensing, motion monitoring, and wound healing; (ii) i-SMD attached on finger, wrist, and elbow for motion sensing. Reprinted from John Wiley and Sons, Copyright 2021. (c) Shark tooth-inspired microneedle dressing for intelligent wound management:[151] (i) schematic diagram of shark tooth-inspired microneedle dressing for intelligent wound management including motion sensing, biochemical analysis, and healing; (ii) multifunctional microneedle dressing integrated with microfluidic channels and flexible electrodes and fabrication process of the origami multifunctional chip; (iii) motion sensing on the microneedle dressing. Reprinted from the American Chemical Society, Copyright 2021.

Published on 03 mai 2023. Downloaded on 05.06.2026 15:09:01.

In a study by Zhang *et al.*, as shown in Fig. 7, the use of MNs for scar treatment was found to be effective through mechanical force modulation.[134] The study involved the preparation of MN arrays with varying densities, with 5 × 5, 10 × 10, and 15 × 15 arrays utilized for scar treatment. Results showed the thickness of scars decreased with the MN intervention, and the effect was more pronounced as the array density increased. Through cellular experiments and histological analysis, the investigators found that MNs reduced the contraction and mechanical stress produced by fibroblasts, resulting in a decrease in the expression of the mechanosensitive gene $ANKRD_1$. Specifically, SF MNs attenuated integrin-FAK signaling, thereby downregulating the expression of TGF-β1, α-SMA, collagen I, and fibronectin to create a low-stress microenvironment that significantly reduced scar formation (Table 3).

2.5 Microneedles for wound monitoring

The assessment of wound healing is a critical component in ensuring optimal therapeutic outcomes.[140] Currently, wound evaluation is primarily based on visual inspection of size, color, and exudate, leading to suboptimal utilization of clinical resources and potential harm to the patient through misdiagnosis.[141,142] The wound-healing process is a dynamic and intricate multistage phenomenon, accompanied by changes in various physiological signals, such as pH, temperature, metabolites produced by microorganisms, and signaling factors secreted by the immune system.[143–146] The state of wound healing can be more accurately assessed by monitoring changes in these physiological markers in real time. Several studies have explored incorporating sensors into excipients for this purpose, with MNs emerging as a promising approach due to their ability to bypass interference from biofilms and crusts at the wound site and enhance detection sensitivity through direct contact with interstitial fluid.[147] A novel colorimetric MN patch incorporating a ligated polymeric nano enzyme has been developed by Shan *et al.*[148] The nano enzyme, formed through ligating Fe ions with gallic acid, displays pH-dependent catalytic activity. The color of the MN patch changes upon alteration in pH and elevation of H_2O_2 concentration, thereby allowing for real-time monitoring of wound status. Furthermore, the liganded polymeric nano enzyme catalyzes the formation of ROS from H_2O_2, thus inactivating bacterial pathogens.

Some strenuous movements at the wound site can interfere with wound recovery, but the patient is often unaware of this. When such strenuous stretching occurs frequently, the wound may face long-term difficulties in healing. Shao *et al.* have designed a near-infrared light-responsive MNs scaffold utilizing 3D printing technology (Fig. 8a).[149] The scaffold consists of a hydrogel precursor, comprising polyurethane, aloe vera gel, and recombinant spidroin, doped with the conductive and photothermal material MXene. The MN body features an inverse opal photonic crystal structure, while the backing layer exhibits a mesh structure, both of which enhance the drug-carrying capacity. To enable infrared light-responsive drug release, mupirocin (an antibiotic) and hEGF are encapsulated in temperature-responsive NIPAM, and release is triggered through photothermal conversion of MXene upon exposure to infrared light. The conductive properties of MXene, which is composed of a two-dimensional multilayer nanosheet structure, enable efficient ion motion and high electrical conductivity. The MNs are fixed on the finger and wrist joints to monitor the electrical resistance response signal during movement. The hydrogel-wrapped MXene is applied to the wound and the electrical resistance is monitored in response to stretching, allowing for the detection of different degrees of bending with good reproducibility.

Gao *et al.* expanded upon Shao's work by introducing a biomarker detection device into the MN patch (Fig. 8b).[150] The conductive medium was replaced with graphene to create a microelectronic circuit capable of detecting the movement of the wound area. The MN array was equipped with four detection areas, which were able to detect the biomarkers IL-6 and CRP in tissue fluid through the use of a double antibody sandwich method and a photonic crystal structure to amplify the signal. As shown in Fig. 8c, to detect the movement of the wound site more stably, Guo *et al.* designed the MN body structure inspired by shark teeth to tilt to the middle at a certain angle, which in turn provides stronger adhesion for the MN detection device to avoid dislodging during repeated movements that may affect the sensitivity of the detection.[151] In addition, since the integration of multiple detection devices into a single patch usually results in a large patch area, which may lead to discomfort in wearing, the researchers employed origami technology to reduce the patch area and increase its versatility. The MN dressing was tested on volunteers and the results showed a high correlation between the regularity of resistance changes and the behavioral state of the volunteers, demonstrating the highly sensitive motion-sensing capability of the MN dressing.

3. Conclusion and future perspective

Wound recovery is a significant public health challenge, and existing treatment modalities are diverse due to the complex nature of wound healing. MN technology has shown promise in improving drug delivery efficiency in wound treatment, as well as enhancing wound-detection sensitivity and accuracy. Furthermore, the unique structure of MNs allows for multifunctionality and programmed drug release, potentially improving drug stability. This paper describes the application of MNs in wound healing in recent years, classified according to the different functions they achieve in wound healing. These studies have all yielded optimistic results in wound healing, demonstrating the advantages and great promise of MNs for wound healing.

Despite these advances, challenges remain in utilizing MNs as a primary tool for wound treatment. One persistent issue is the limited drug dose delivered. Additionally, MNs' penetration is typically vertical, making it difficult to achieve complete penetration in uneven wound sites. Although some

 This journal is © The Royal Society of Chemistry 2023

Published on 03 mai 2023. Downloaded on 05.06.2026 15:09:01.

studies have explored flexible materials to enable drug delivery in curved locations, penetration efficiency is often limited in complex wounds. To date, research on MNs for wound treatment has been mainly at the animal experimental stage, and MNs could easily cover wounds in rats completely; one problem that must be faced to achieve clinical conversion is the large area of wounds, where it is difficult to achieve high efficacy with a smaller MN area.

In addition, wound healing is a complex process, especially the conversion of the inflammatory phase to the proliferative phase, which involves the conversion of immune cells from a pro-inflammatory to an anti-inflammatory type. Therefore, the treatment of wounds cannot be simply targeted at a certain stage and cannot simply deliver multiple drugs at the same time. The correct treatment modality should be achieved by giving targeted treatment regimens at different stages. However, in the process of wound-healing self-management, it is difficult for people to distinguish the current state of the wound except during the hemostasis period, and it is difficult to make timely and accurate judgments for treatment. Therefore, there is a more intelligent and multi-functional requirement for wound treatment with MNs. One idea is to achieve real-time monitoring of wound status, with more than one signal molecule measurement, involving the measurement of multiple signal factors throughout the wound-healing process, giving patients timely information and feedback for accurate treatment. In such a system, an intelligent drug-delivery system could be equipped to realize the unification of collecting signals and giving feedback. Another idea will be to realize intelligent drug delivery by MNs, *i.e.* responsive drug delivery, integrating multiple drug-delivery systems on one MN to realize responsive drug delivery under different physiological signal stimulations. Whether it is wound-signal monitoring or wound-intelligent responsive drug delivery, there has been a lot of related research, but the difficulty lies in how to diversify and integrate the detection signals and drug delivery systems into the small area of an MN. In addition, cell therapy has been a promising therapy for many diseases, and delivering cells is not just about achieving a single aspect of treatment. Cells are dynamic in their involvement in the treatment process, and can dynamically adapt the treatment to the environment; how to use this feature for complex therapeutic processes in wounds is also a research direction for MNs for cell delivery. In this research, MNs have to be coordinated between maintaining cell viability and mechanical properties, which involves the adjustment of MN materials and the design of structures, which is also a difficult problem. Solving these problems could greatly expand the application of MNs in wound healing and accelerate clinical conversion. Overall, MN is a very promising management modality for wound healing. This article reviews recent work on MNs for wound management and presents difficulties and perspectives on the future of MNs for wound management, hoping to inspire more relevant research and provide more intelligent and effective solutions for wound management.

Author contributions

X. D. G., M. A. S. and B. Z. C. conceived the idea and designed this paper; L. L. and Y. L. J. assisted in drawing of related images; Y. L. and Y. H. Z. assisted in collecting relevant literature; Z. Q. Z. wrote and revised the manuscript.

Conflicts of interest

There are no conflicts to declare.

Acknowledgements

This work was financially supported by the National Natural Science Foundation of China (52161145410), China Postdoctoral Science Foundation (2022M720372), Iran National Science Foundation-National Natural Science Foundation of China joint grant (No. 4001987), and the long-term subsidy mechanism from the Ministry of Finance and the Ministry of Education of PRC. Prof. Shahbazi acknowledges the financial support of the incentive fund from the University of Groningen, Groningen, The Netherlands.

References

1 S. Vijayavenkataraman, W. Lu and J. Fuh, *Biofabrication*, 2016, **8**, 032001.
2 M. Takeo, W. Lee and M. Ito, *Cold Spring Harbor Perspect. Med.*, 2015, **5**, a023267.
3 G. Sun, Y. I. Shen and J. W. Harmon, *Adv. Healthcare Mater.*, 2018, **7**, 1800016.
4 S. Lu, X. Zhang, Z. Tang, H. Xiao, M. Zhang, K. Liu, L. Chen, L. Huang, Y. Ni and H. Wu, *Chem. Eng. J.*, 2021, **417**, 129329.
5 L. Yao, H. Gao, Z. Lin, Q. Dai, S. Zhu, S. Li, C. Liu, Q. Feng, Q. Li and G. Wang, *Chem. Eng. J.*, 2022, **428**, 131005.
6 S. a. Guo and L. A. DiPietro, *J. Dent. Res.*, 2010, **89**, 219–229.
7 K. Izadi and P. Ganchi, *Clin. Plast. Surg.*, 2005, **32**, 209–222.
8 S. A. Eming, P. Martin and M. Tomic-Canic, *Sci. Transl. Med.*, 2014, **6**, 265sr266–265sr266.
9 M. Farahani and A. Shafiee, *Adv. Healthcare Mater.*, 2021, **10**, 2100477.
10 J. G. Powers, C. Higham, K. Broussard and T. J. Phillips, *J. Am. Acad. Dermatol.*, 2016, **74**, 607–625.
11 S. Enoch and D. J. Leaper, *Surgery*, 2008, **26**, 31–37.
12 S. Singh, A. Young and C.-E. McNaught, *Surgery*, 2017, **35**, 473–477.
13 S. Pourshahrestani, E. Zeimaran, N. A. Kadri, N. Mutlu and A. R. Boccaccini, *Adv. Healthcare Mater.*, 2020, **9**, 2000905.

Published on 03 mai 2023. Downloaded on 05.06.2026 15:09:01.

14 E. A. Gantwerker and D. B. Hom, *Clin. Plast. Surg.*, 2012, **39**, 85–97.
15 O. Richard, C. Chollet-Xemard and B. Vivien, *JAMA Surg.*, 2021, **156**, 101–101.
16 T. J. Koh and L. A. DiPietro, *Expert Rev. Mol. Med.*, 2011, **13**, e23.
17 S. Q. Zhang, Y. Y. Liu, X. Zhang, D. S. Zhu, X. Qi, X. C. Cao, Y. H. Fang, Y. Z. Che, Z. C. Han and Z. X. He, *Theranostics*, 2018, **8**, 5348.
18 T. A. Wilgus, *Pharmacol. Res.*, 2008, **58**, 112–116.
19 P. Bainbridge, *J. Wound Care*, 2013, **22**, 407–412.
20 T. Su, Y. Z. Xiao, Y. Xiao, Q. Guo, C. J. Li, Y. Huang, Q. F. Deng, J. X. Wen, F. L. Zhou and X. H. Luo, *ACS Nano*, 2019, **13**, 2450–2462.
21 S. Chen, M. Zhang, X. Shao, X. Wang, L. Zhang, P. Xu, W. Zhong, L. Zhang, M. Xing and L. Zhang, *J. Mater. Chem. B*, 2015, **3**, 6798–6804.
22 L. Zhou, W. Pi, S. Cheng, Z. Gu, K. Zhang, T. Min, W. Zhang, H. Du, P. Zhang and Y. Wen, *Adv. Funct. Mater.*, 2021, **31**, 2106167.
23 B. Guo, R. Dong, Y. Liang and M. Li, *Nat. Rev. Chem.*, 2021, **5**, 773–791.
24 P. Rousselle, F. Braye and G. Dayan, *Adv. Drug Delivery Rev.*, 2019, **146**, 344–365.
25 S. Nam and D. Mooney, *Chem. Rev.*, 2021, **121**, 11336–11384.
26 E. R. Zielins, E. A. Brett, A. Luan, M. S. Hu, G. G. Walmsley, K. Paik, K. Senarath-Yapa, D. A. Atashroo, T. Wearda and H. P. Lorenz, *Expert Opin. Emerging Drugs*, 2015, **20**, 235–246.
27 L. Hall-Stoodley, J. W. Costerton and P. Stoodley, *Nat. Rev. Microbiol.*, 2004, **2**, 95–108.
28 C. De la Fuente-Núñez, F. Reffuveille, L. Fernández and R. E. Hancock, *Curr. Opin. Microbiol.*, 2013, **16**, 580–589.
29 S. L. Percival, *Wounds*, 2004, **16**, 234–240.
30 S. Reuter, S. C. Gupta, M. M. Chaturvedi and B. B. Aggarwal, *Free Radicals Biol. Med.*, 2010, **49**, 1603–1616.
31 G. Waris and H. Ahsan, *J. Carcinog.*, 2006, **5**, 14.
32 R. Dong and B. Guo, *Nano Today*, 2021, **41**, 101290.
33 X. F. Li, P. p. Lu, H. R. Jia, G. F. Li, B. F. Zhu, X. Wang and F. G. Wu, *Coord. Chem. Rev.*, 2023, **475**, 214823.
34 A. Mohandas, S. Deepthi, R. Biswas and R. Jayakumar, *Bioact. Mater.*, 2018, **3**, 267–277.
35 C. Dhand, M. Venkatesh, V. A. Barathi, S. Harini, S. Bairagi, E. G. T. Leng, N. Muruganandham, K. Z. W. Low, M. H. U. T. Fazil and X. J. Loh, *Biomaterials*, 2017, **138**, 153–168.
36 H. Hamedi, S. Moradi, S. M. Hudson and A. E. Tonelli, *Carbohydr. Polym.*, 2018, **199**, 445–460.
37 O. Catanzano, F. Quaglia and J. S. Boateng, *Expert Opin. Drug Delivery*, 2021, **18**, 737–759.
38 Q. Zeng, X. Qi, G. Shi, M. Zhang and H. Haick, *ACS Nano*, 2022, **16**, 1708–1733.
39 N. Thet, D. Alves, J. Bean, S. Booth, J. Nzakizwanayo, A. Young, B. V. Jones and A. T. A. Jenkins, *ACS Appl. Mater. Interfaces*, 2016, **8**, 14909–14919.
40 C. Xu, O. U. Akakuru, X. Ma, J. Zheng, J. Zheng and A. Wu, *Bioconjugate Chem.*, 2020, **31**, 1708–1723.
41 G. C. Gurtner, S. Werner, Y. Barrandon and M. T. Longaker, *Nature*, 2008, **453**, 314–321.
42 H. Derakhshandeh, F. Aghabaglou, A. McCarthy, A. Mostafavi, C. Wiseman, Z. Bonick, I. Ghanavati, S. Harris, C. Kreikemeier-Bower and S. M. Moosavi Basri, *Adv. Funct. Mater.*, 2020, **30**, 1905544.
43 Z. Q. Zhao, L. Liang, L. F. Hu, Y. T. He, L. Y. Jing, Y. Liu, B. Z. Chen and X. D. Guo, *Biomacromolecules*, 2022, **23**, 5330–5339.
44 B. Z. Chen, L. Q. Zhang, Y. Y. Xia, X. P. Zhang and X. D. Guo, *Sci. Adv.*, 2020, **6**, eaba7260.
45 X. Jin, D. D. Zhu, B. Z. Chen, M. Ashfaq and X. D. Guo, *Adv. Drug Delivery Rev.*, 2018, **127**, 119–137.
46 Y. Xu, X. Y. Wu, X. X. Zhang, Y. Zu, Q. Tan and Y. J. Zhao, *Adv. Funct. Mater.*, 2023, **33**, 2209986.
47 B. Z. Chen, J. L. Liu, Q. Y. Li, Z. N. Wang, X. P. Zhang, C. B. Shen, Y. Cui and X. D. Guo, *ACS Appl. Bio Mater.*, 2019, **2**, 5616–5625.
48 F. Damiri, N. Kommineni, S. O. Ebhodaghe, R. Bulusu, V. G. S. S. Jyothi, A. A. Sayed, A. A. Awaji, M. O. Germoush, H. S. Al-Malky, M. Z. Nasrullah, M. H. Rahman, M. M. Abdel-Daim and M. Berrada, *Pharmaceuticals*, 2022, **15**, 190.
49 J. H. Jung and S. G. Jin, *J. Pharm. Invest.*, 2021, **51**, 503–517.
50 R. Jamaledin, C. K. Y. Yiu, E. N. Zare, L.-N. Niu, R. Vecchione, G. Chen, Z. Gu, F. R. Tay and P. Makvandi, *Adv. Mater.*, 2020, **32**, 2002129.
51 K. A. S. Al-Japairai, S. Mahmood, S. H. Almurisi, J. R. Venugopal, A. R. Hilles, M. Azmana and S. Raman, *Int. J. Pharm.*, 2020, **587**, 119673.
52 J. Yang, X. Liu, Y. Fu and Y. Song, *Acta Pharm. Sin. B*, 2019, **9**, 469–483.
53 A. H. Sabri, J. Ogilvie, K. Abdulhamid, V. Shpadaruk, J. McKenna, J. Segal, D. J. Scurr and M. Marlow, *Eur. J. Pharm. Biopharm.*, 2019, **140**, 121–140.
54 M. R. Prausnitz, J. A. Mikszta, M. Cormier and A. K. Andrianov, *Vaccines for Pandemic Influenza*, 2009, vol. 333, pp. 369–393.
55 I. Menon, P. Bagwe, K. B. Gomes, L. Bajaj, R. Gala, M. N. Uddin, M. J. D'souza and S. M. Zughaier, *Micromachines*, 2021, **12**, 435.
56 X. Chen, L. Wang, H. Yu, C. Li, J. Feng, F. Haq, A. Khan and R. U. Khan, *J. Controlled Release*, 2018, **288**, 173–188.
57 B. Z. Chen, Y. Yang, B. B. Wang, M. Ashfaq and X. D. Guo, *Int. J. Pharm.*, 2019, **556**, 338–348.
58 B. Z. Chen, Z. Q. Zhao, M. A. Shahbazi and X. D. Guo, *Nanoscale Horiz.*, 2022, **7**, 715–728.
59 F. Q. Luo, G. J. Chen, W. Xu, D. J. Zhou, J. X. Li, Y. C. Huang, R. Lin, Z. Gu and J. Z. Du, *Nano Res.*, 2021, **14**, 2689–2696.
60 J. Wang, Z. Wang, J. Yu, A. R. Kahkoska, J. B. Buse and Z. Gu, *Adv. Mater.*, 2020, **32**, 1902004.
61 Y. Yang, B. Z. Chen, X. P. Zhang, H. Zheng, Z. Li, C. Y. Zhang and X. D. Guo, *ACS Appl. Mater. Interfaces*, 2022, **14**, 31645–31654.

 This journal is © The Royal Society of Chemistry 2023

Published on 03 mai 2023. Downloaded on 05.06.2026 15:09:01.

62 R. Jamaledin, P. Makvandi, C. K. Yiu, T. Agarwal, R. Vecchione, W. Sun, T. K. Maiti, F. R. Tay and P. A. Netti, *Adv. Ther.*, 2020, **3**, 2000171.
63 Y. Zhao, Y. Zhou, D. Yang, X. Gao, T. Wen, J. Fu, X. Wen, G. Quan, X. Pan and C. Wu, *Acta Biomater.*, 2021, **135**, 164–178.
64 H. Zhu, H. Chen, X. Zeng, Z. Wang, X. Zhang, Y. Wu, Y. Gao, J. Zhang, K. Liu and R. Liu, *Biomaterials*, 2014, **35**, 2391–2400.
65 M. C. He, B. Z. Chen, M. Ashfaq and X. D. Guo, *Drug Delivery Transl. Res.*, 2018, **8**, 1034–1042.
66 M. R. Prausnitz, Y. Gomaa and W. Li, *Nat. Med.*, 2019, **25**, 1471–1472.
67 J. Tang, J. Wang, K. Huang, Y. Ye, T. Su, L. Qiao, M. T. Hensley, T. G. Caranasos, J. Zhang and Z. Gu, *Sci. Adv.*, 2018, **4**, eaat9365.
68 J. W. Lee and M. R. Prausnitz, *Expert Opin. Drug Delivery*, 2018, **15**, 541–543.
69 Z. Wang, Z. Yang, J. Jiang, Z. Shi, Y. Mao, N. Qin and T. H. Tao, *Adv. Mater.*, 2022, **34**, 2106606.
70 Y. Zeng, J. Wang, Z. Wang, G. Chen, J. Yu, S. Li, Q. Li, H. Li, D. Wen and Z. Gu, *Nano Today*, 2020, **35**, 100984.
71 J. Gao, W. Huang, Z. Chen, C. Yi and L. Jiang, *Sens. Actuators, B*, 2019, **287**, 102–110.
72 R. He, H. Liu, T. Fang, Y. Niu, H. Zhang, F. Han, B. Gao, F. Li and F. Xu, *Adv. Sci.*, 2021, **8**, 2103030.
73 C. Kolluru, M. Williams, J. Chae and M. R. Prausnitz, *Adv. Healthcare Mater.*, 2019, **8**, 1801262.
74 D. Han, R. S. Morde, S. Mariani, A. A. La Mattina, E. Vignali, C. Yang, G. Barillaro and H. Lee, *Adv. Funct. Mater.*, 2020, **30**, 1909197.
75 E. Y. Jeon, J. Lee, B. J. Kim, K. I. Joo, K. H. Kim, G. Lim and H. J. Cha, *Biomaterials*, 2019, **222**, 119439.
76 J. Lee, S. Park, P. T. Le, G. Lee, H. W. Lee, G. Yun, J. Jeon, J. Park, D. T. Pham, Y. S. Park, H. Lim, C. Kim, T. S. Hwang, S. W. Kim and G. Lim, *Adv. Healthcare Mater.*, 2023, 2201697.
77 C. M. Gibson, R. Mehran, C. Bode, J. Halperin, F. W. Verheugt, P. Wildgoose, M. Birmingham, J. Ianus, P. Burton and M. Van Eickels, *N. Engl. J. Med.*, 2016, **375**, 2423–2434.
78 D. A. Hickman, C. L. Pawlowski, U. D. Sekhon, J. Marks and A. S. Gupta, *Adv. Mater.*, 2018, **30**, 1700859.
79 A. Pathak, R. Zhao, D. Monroe, H. Roberts, B. Sheridan, C. Selzman and G. Stouffer, *J. Thromb. Haemostasis*, 2006, **4**, 60–67.
80 M. Hoffman, *J. Thromb. Thrombolysis*, 2003, **16**, 17–20.
81 A. Duarte, J. Coelho, J. Bordado, M. Cidade and M. Gil, *Prog. Polym. Sci.*, 2012, **37**, 1031–1050.
82 L. Al-Mubarak and M. Al-Haddab, *J. Cutan. Aesthet. Surg.*, 2013, **6**, 178.
83 H. A. Scheraga, *Biophys. Chem.*, 2004, **112**, 117–130.
84 R. Haghniaz, H. J. Kim, H. Montazerian, A. Baidya, M. Tavafoghi, Y. Chen, Y. Zhu, S. Karamikamkar, A. Sheikhi and A. Khademhosseini, *Bioact. Mater.*, 2023, **23**, 314–327.
85 X. X. Zhang, G. P. Chen, L. J. Cai, Y. T. Wang, L. Y. Sun and Y. J. Zhao, *Chem. Eng. J.*, 2021, **414**, 128905.
86 M. Malone, T. Bjarnsholt, A. J. McBain, G. A. James, P. Stoodley, D. Leaper, M. Tachi, G. Schultz, T. Swanson and R. D. Wolcott, *J. Wound Care*, 2017, **26**, 20–25.
87 T. Bjarnsholt, T. Eberlein, M. Malone and G. Schultz, *Wounds Int.*, 2017, **8**, 1–6.
88 B. F. Gilmore, P. B. Flynn, S. O'Brien, N. Hickok, T. Freeman and P. Bourke, *Trends Biotechnol.*, 2018, **36**, 627–638.
89 K. R. Sims, Y. Liu, G. Hwang, H. I. Jung, H. Koo and D. S. Benoit, *Nanoscale*, 2019, **11**, 219–236.
90 M. S. Arshad, A. T. Zahra, S. Zafar, H. Zaman, A. Akhtar, M. M. Ayaz, I. Kucuk, M. Maniruzzaman, M.-W. Chang and Z. Ahmad, *Pharm. Res.*, 2021, **38**, 165–177.
91 S. Y. Park, H. U. Lee, Y. C. Lee, G. H. Kim, E. C. Park, S. H. Han, J. G. Lee, S. Choi, N. S. Heo, D. L. Kim, Y. S. Huh and J. Lee, *Mater. Sci. Eng., C*, 2014, **42**, 757–762.
92 G. H. Frydman, D. Olaleye, D. Annamalai, K. Layne, I. Yang, H. M. A. Kaafarani and J. G. Fox, *Sci. Rep.*, 2020, **10**, 13229.
93 X. X. Yu, C. X. Wang, Y. F. Wang, L. H. Li, X. Gao, T. T. Zhu, P. G. An, Z. J. Meng, W. C. Wang, T. Wu and Y. P. Hao, *Front. Chem.*, 2022, **10**, 838920.
94 C. W. Hall and T. F. Mah, *FEMS Microbiol. Rev.*, 2017, **41**, 276–301.
95 J. L. Balcázar, J. Subirats and C. M. Borrego, *Front. Microbiol.*, 2015, **6**, 1216.
96 Y. J. Su, V. L. Mainardi, H. J. Wang, A. McCarthy, Y. S. Zhang, S. X. Chen, J. V. John, S. L. Wong, R. R. Hollins, G. S. Wang and J. W. Xie, *ACS Nano*, 2020, **14**, 11775–11786.
97 Y. Su, A. McCarthy, S. L. Wong, R. R. Hollins, G. Wang and J. Xie, *Adv. Healthcare Mater.*, 2021, **10**, 2100135.
98 A. Sirelkhatim, S. Mahmud, A. Seeni, N. H. M. Kaus, L. C. Ann, S. K. M. Bakhori, H. Hasan and D. Mohamad, *Nano-Micro Lett.*, 2015, **7**, 219–242.
99 S. Yao, J. Chi, Y. Wang, Y. Zhao, Y. Luo and Y. Wang, *Adv. Healthcare Mater.*, 2021, **10**, e2100056.
100 Y. Deng, C. Yang, Y. Y. Zhu, W. Y. Liu, H. L. Li, L. P. Wang, W. Chen, Z. Wang and L. Wang, *Nano Lett.*, 2022, **22**, 2702–2711.
101 Y. Sun, J. Liu, H. Wang, S. Li, X. Pan, B. Xu, H. Yang, Q. Wu, W. Li, X. Su, Z. Huang, X. Guo and H. Liu, *Adv. Funct. Mater.*, 2021, **31**, 2100218.
102 A. Ullah, M. Jang, H. Khan, H. J. Choi, S. An, D. Kim, Y. R. Kim, U. K. Kim and G. M. Kim, *Sens. Actuators, B*, 2021, **345**, 130441.
103 M. Mir, A. D. Permana, N. Ahmed, G. M. Khan, A. U. Rehman and R. F. Donnelly, *Eur. J. Pharm. Biopharm.*, 2020, **147**, 57–68.
104 X. L. Lei, M. J. Li, C. Wang, P. F. Cui, L. Qiu, S. W. Zhou, P. J. Jiang, H. H. Li, D. H. Zhao, X. Y. Ni, J. H. Wang and J. Xia, *Int. J. Biol. Macromol.*, 2022, **217**, 55–65.

Published on 03 mai 2023. Downloaded on 05.06.2026 15:09:01.

105 E. Caffarel-Salvador, M.-C. Kearney, R. Mairs, L. Gallo, S. A. Stewart, A. J. Brady and R. F. Donnelly, *Pharmaceutics*, 2015, **7**, 397–412.
106 X. Yang, M. Q. Jia, Z. Li, Z. H. Ma, J. Y. Lv, D. W. N. Jia, D. F. He, R. Zeng, G. X. Luo and Y. L. Yu, *Int. J. Biol. Macromol.*, 2022, **215**, 550–559.
107 H. K. Kao, B. Chen, G. F. Murphy, Q. Li, D. P. Orgill and L. Guo, *Ann. Surg.*, 2011, **254**, 1066–1074.
108 K. Lee, Y. M. Xue, J. Lee, H. J. Kim, Y. W. Liu, P. Tebon, E. Sarikhani, W. J. Sun, S. M. Zhang, R. Haghniaz, B. Celebi-Saltik, X. W. Zhou, S. Ostrovidov, S. Ahadian, N. Ashammakhi, M. R. Dokmeci and A. Khademhosseini, *Adv. Funct. Mater.*, 2020, **30**, 2000086.
109 M. T. Yin, J. Y. Z. Wu, M. W. Deng, P. Wang, G. Y. Ji, M. S. Wang, C. H. Zhou, N. T. Blum, W. J. Zhang, H. L. Shi, N. Q. Jia, X. S. Wang and P. Huang, *ACS Nano*, 2021, **15**, 17842–17853.
110 X. X. Zhang, G. P. Chen, Y. X. Liu, L. Y. Sun, L. Y. Sun and Y. J. Zhao, *ACS Nano*, 2020, **14**, 5901–5908.
111 X. X. Zhang, G. P. Chen, L. Y. Sun, F. F. Ye, X. Shen and Y. J. Zhao, *Chem. Eng. J.*, 2021, **406**, 126741.
112 Y. Shan, B. W. Tan, M. Zhang, X. Xie and J. F. Liao, *J. Nanobiotechnol.*, 2022, **20**, 238.
113 G. P. Guan, Q. Zhang, Z. Z. Jiang, J. Liu, J. J. Wan, P. Jin and Q. Z. Lv, *Small*, 2022, **18**, e2203064.
114 S. Yao, Y. T. Wang, J. J. Chi, Y. R. Yu, Y. J. Zhao, Y. Luo and Y. G. Wang, *Adv. Sci.*, 2022, **9**, 2103449.
115 J. J. Chi, L. Y. Sun, L. J. Cai, L. Fan, C. M. Shao, L. R. Shang and Y. J. Zhao, *Bioact. Mater.*, 2021, **6**, 3507–3514.
116 Q. Lei, D. F. He, L. P. Ding, F. H. Kong, P. Y. He, J. D. Huang, J. M. Guo, C. J. Brinker, G. X. Luo, W. Zhu and Y. L. Yu, *Adv. Funct. Mater.*, 2022, **32**, 2113269.
117 T. Q. Ning, F. H. Yang, D. L. Chen, Z. Z. Jia, R. Q. Yuan, Z. Q. Du, S. Y. Liu, Y. Yu, X. C. Dai, X. F. Niu and Y. B. Fan, *Adv. Healthcare Mater.*, 2021, **11**, e2102180.
118 Y. A. Xue, C. Chen, R. Tan, J. Y. Zhang, Q. Fang, R. Jin, X. Y. Mi, D. Y. Sun, Y. A. Xue, Y. Wang, R. Xiong, H. J. Lu and W. Q. Tan, *ACS Appl. Mater. Interfaces*, 2022, **14**, 37396–37409.
119 J. J. Gan, X. X. Zhang, W. J. Ma, Y. J. Zhao and L. Y. Sun, *Nano Today*, 2022, **47**, 101630.
120 W. J. Ma, X. X. Zhang, Y. X. Liu, L. Fan, J. J. Gan, W. L. Liu, Y. J. Zhao and L. Y. Sun, *Adv. Sci.*, 2022, **9**, 2103317.
121 J. J. Chi, X. X. Zhang, C. W. Chen, C. M. Shao, Y. J. Zhao and Y. G. Wang, *Bioact. Mater.*, 2020, **5**, 253–259.
122 L. Y. Sun, L. Fan, F. K. Bian, G. P. Chen, Y. T. Wang and Y. J. Zhao, *Research*, 2021, **2021**, 9838490.
123 Y. Wang, H. Lu, M. Guo, J. Chu, B. Gao and B. He, *Adv. Healthcare Mater.*, 2021, **11**, 2101659.
124 L. Y. Long, W. Q. Liu, L. Li, C. Hu, S. Y. He, L. Lu, J. Wang, L. Yang and Y. B. Wang, *Nanoscale*, 2022, **14**, 1285–1295.
125 M. Yuan, K. Liu, T. Jiang, S. B. Li, J. Chen, Z. H. Wu, W. Q. Li, R. Z. Tan, W. Y. Wei, X. F. Yang, H. L. Dai and Z. B. Chen, *J. Nanobiotechnol.*, 2022, **20**, 147.
126 Z. Y. Zeng, G. H. Jiang, Y. F. Sun, U. E. Aharodnikau, K. E. Yunusov, X. F. Gao, T. Q. Liu and S. O. Solomevich, *Biomater. Sci.*, 2022, **10**, 5326–5339.
127 P. H. Wang, Y. J. Pu, Y. H. Ren, W. H. Kong, L. L. Xu, W. J. Zhang, T. Q. Shi, J. P. Ma, S. Li, X. Y. Tan and B. Chi, *Int. J. Biol. Macromol.*, 2023, **226**, 813–822.
128 C. C. Finnerty, M. G. Jeschke, L. K. Branski, J. P. Barret, P. Dziewulski and D. N. Herndon, *Lancet*, 2016, **388**, 1427–1436.
129 M. Gholipourmalekabadi, S. Khosravimelal, Z. Nokhbedehghan, M. Sameni, V. Jajarmi, A. M. Urbanska, H. Mirzaei, M. Salimi, N. P. S. Chauhan and M. Mobaraki, *ACS Biomater. Sci. Eng.*, 2019, **5**, 1487–1496.
130 N. Zhang, L. P. Xue, A. Younas, F. F. Liu, J. H. Sun, Z. L. Dong and Y. X. Zhao, *Carbohydr. Polym.*, 2022, **284**, 119219.
131 B. B. Yang, Y. T. Dong, Y. F. Shen, A. L. Hou, G. L. Quan, X. Pan and C. B. Wu, *Bioact. Mater.*, 2021, **6**, 2400–2411.
132 T. Wu, X. L. Hou, J. Q. Li, H. Ruan, L. X. Pei, T. Guo, Z. Wang, T. Y. Ci, S. Y. Ruan, Y. Z. He, Z. H. He, N. P. Feng and Y. T. Zhang, *ACS Nano*, 2021, **15**, 20087–20104.
133 Y. Huang, T. T. Peng, W. S. Hu, X. Y. Gao, Y. Y. Chen, Q. Zhang, C. B. Wu and X. Pan, *J. Controlled Release*, 2022, **343**, 408–419.
134 Q. Zhang, L. Shi, H. He, X. M. Liu, Y. Huang, D. Xu, M. Y. Yao, N. Zhang, Y. C. Guo, Y. F. Lu, H. S. Li, J. Y. Zhou, J. L. Tan, M. Xing and G. X. Luo, *ACS Nano*, 2022, **16**, 10163–10178.
135 S. Q. Lin, G. L. Quan, A. L. Hou, P. P. Yang, T. T. Peng, Y. K. Gu, W. B. Qin, R. B. Liu, X. Y. Ma, X. Pan, H. Liu, L. L. Wang and C. B. Wu, *J. Controlled Release*, 2019, **306**, 69–82.
136 X. Y. Ning, C. Wiraja, W. T. S. Chew, C. Fan and C. J. Xu, *Acta Pharm. Sin. B*, 2021, **11**, 2937–2944.
137 J. Park and Y. C. Kim, *Drug Delivery Transl. Res.*, 2021, **11**, 205–213.
138 P. N. Chien, J. H. Jeong, S. Y. Nam, S. Y. Lim, N. V. Long, X. R. Zhang, J. H. Jeong and C. Y. Heo, *In Vivo*, 2022, **36**, 1734–1744.
139 Y. Y. Chun, W. W. R. Tan, M. I. G. Vos, W. K. Chan, H. L. Tey, N. S. Tan and T. T. Y. Tan, *Biomater. Sci.*, 2022, **10**, 3963–3971.
140 A. Kekonen, M. Bergelin, M. Johansson, N. Kumar Joon, J. Bobacka and J. Viik, *Sensors*, 2019, **19**, 2505.
141 Z. Peles, I. Binderman, I. Berdicevsky and M. Zilberman, *J. Tissue Eng. Regener. Med.*, 2013, **7**, 401–412.
142 J. J. Elsner, A. Shefy-Peleg and M. Zilberman, *J. Biomed. Mater. Res., Part B*, 2010, **93**, 425–435.
143 S. Ono, R. Imai, Y. Ida, D. Shibata, T. Komiya and H. Matsumura, *Burns*, 2015, **41**, 820–824.
144 Y. Y. Broza, X. Zhou, M. Yuan, D. Qu, Y. Zheng, R. Vishinkin, M. Khatib, W. Wu and H. Haick, *Chem. Rev.*, 2019, **119**, 11761–11817.
145 M. L. Fernandez, Z. Upton, H. Edwards, K. Finlayson and G. K. Shooter, *Int. Wound J.*, 2012, **9**, 139–149.

 This journal is © The Royal Society of Chemistry 2023

146 A. Daneshkhah, A. P. Siegel and M. Agarwal, in *Wound Healing, Tissue Repair, and Regeneration in Diabetes*, Elsevier, 2020, pp. 491–512.
147 B. L. Zhang, X. P. Zhang, B. Z. Chen, W. M. Fei, Y. Cui and X. D. Guo, *Microchem. J.*, 2021, **162**, 105830.
148 J. Y. Shan, X. X. Zhang, B. Kong, Y. J. Zhu, Z. X. Gu, L. J. Ren and Y. J. Zhao, *Chem. Eng. J.*, 2022, **444**, 136640.
149 Y. Shao, K. Y. Dong, X. Y. Lu, B. B. Gao and B. F. He, *ACS Appl. Mater. Interfaces*, 2022, **14**, 56525–56534.
150 B. Gao, M. Guo, K. Lyu, T. Chu and B. He, *Adv. Funct. Mater.*, 2021, **31**, 2006839.
151 M. Z. Guo, Y. Q. Wang, B. B. Gao and B. F. He, *ACS Nano*, 2021, **15**, 15316–15327.

Published on 03 mai 2023. Downloaded on 05.06.2026 15:09:01.